JOURNAL OF COMPUTATIONAL PHYSICS **146,** 366–403 (1998)
ARTICLE NO. CP986063

Asymptotic Analysis of a Computational Method for Time- and Frequency-Dependent Radiative Transfer

Marvin L. Adams* and Paul F. Nowak†

**Department of Nuclear Engineering, Texas A&M University, College Station, Texas 77843-3133; and*
†Lawrence Livermore National Laboratory, P.O. Box 808, L-18, Livermore, California 94550
E-mail: mladams@tamu.edu and †pnowak@llnl.gov

Received February 12, 1998; revised July 20, 1998

We consider a time-dependent, energy-dependent, nonlinear radiative transfer problem in which opacities are large [$O(\varepsilon^{-1})$] and interior sources are small [$O(\varepsilon)$]. An asymptotic analysis of this problem as $\varepsilon \to 0$ leads to the equilibrium diffusion equation in the interior of the system, along with boundary conditions and initial conditions for this equation. We apply the same asymptotic analysis to a discrete version of the problem, in which the frequency variable is discretized by the multigroup method, the direction variable by the discrete-ordinates method, the time variable by the fully implicit method, and the spatial variable by a subcell-balance method. We find that as $\varepsilon \to 0$ the discrete solution satisfies a robust discretized version of the correct equilibrium diffusion equation, with boundary conditions and initial conditions that are remarkably accurate. The analysis thus predicts that if a spatial grid is chosen that resolves interior temperature gradients, then the numerical method obtains an accurate solution in the interior of the system, even though the optical thickness of the spatial cells tends to ∞ and boundary layers in the transport solution are not resolved. We go a step further to analyze problems that are optically thin at some photon frequencies but thick at others, and show that once again the discrete solution is remarkably accurate. We present numerical results that verify these and other predictions of the analyses.

Key Words: radiative transfer; asymptotic analysis; computational transport; spatial discretization.

I. INTRODUCTION

The motivation for this work is the need to obtain accurate numerical solutions to radiative-transfer problems of practical interest. Often in such problems there are optically thick regions in which absorption and re-emission are the dominant physical processes that

0021-9991/98 $25.00

determine the radiation energy density. Such regions are "diffusive" in the sense that in their interiors the radiation energy density, to leading order, satisfies the "equilibrium" diffusion equation [1].

Most practical radiative-transfer problems cannot be solved analytically and hence require numerical methods. The extreme optical thickness of these problems forces spatial grids to be very coarse, with cells that are thousands of mean-free paths thick (or more) in low-frequency groups. It is therefore important to understand how numerical methods behave in optically thick regions with coarse spatial grids. Many studies have been done on this subject, but most consider a relatively simple problem: linear, steady-state, single frequency group [2–5]. A recent study [6] considered a more realistic problem with an arbitrary number of frequency groups, but it was also linear and steady state. In a very recent development, Morel *et al.* [7] studied a realistic radiative-transfer problem that is nonlinear, time dependent, and frequency dependent. The authors performed an asymptotic analysis of a discrete version of this problem, in which the frequency variable is discretized by the multigroup method, the direction variable by discrete ordinates, the time variable fully implicitly, and the spatial variable by a linear discontinuous finite-element method with mass-matrix lumping (the "lumped linear discontinuous" method, or "LLD"). Their study assumes one-dimensional planar symmetry. Their analysis and numerical results show that the discrete solution is fairly accurate, even when the spatial grid does not resolve boundary layers. This is a remarkable result, because the optical thickness of the spatial cells in these problems tends toward ∞, and transport discretizations are usually known to be accurate only when the optical thickness of spatial cells is much less than unity.

The work we present here complements that of Morel *et al*. The main differences are:

- We introduce the "simple" corner-balance (SCB) method, which is based on enforcing energy conservation on subcells. We describe SCB for an arbitrary grid in two dimensions and show it in detail for planar (slab) geometry.
- In slab geometry, SCB is almost identical to LLD; however, our SCB method uses a different opacity in each subcell, whereas the LLD method analyzed by Morel *et al*. uses a single opacity throughout each cell.
- We present an analysis of the "initial layer," obtaining initial conditions satisfied by the leading-order discrete solution. We compare these against the initial conditions satisfied by the leading-order exact solution and show that they are almost identical.
- We perform a thorough analysis of boundary-layer behavior, using a model opacity to make sharp predictions about the behavior of the SCB, LLD, and exact solutions of problems with different incident photon distributions.
- We analyze problems that are optically thick in some frequency ranges but optically thin in others. This kind of problem is often encountered in practice.
- We manipulate the boundary condition for the leading-order interior solution into a form that is an obvious generalization of that obtained by previous one-group studies.
- We study a wider variety of test problems, including several with wave fronts and with severe boundary layers.

The remainder of this paper is organized as follows. In the next section we describe the problem and summarize what is known about its analytic solution in thick diffusive regions. In Section III we present an SCB method and use it to discretize the radiative-transfer problem. In Section IV we use an asymptotic analysis to show that the SCB solution satisfies, to leading order in thick diffusive regions, a robust and accurate discretization of

the equilibrium diffusion equation. We derive the initial and boundary conditions satisfied by this leading-order solution. This analysis predicts that the SCB scheme will achieve reasonably accurate numerical results inside the physical system even if the grid does not resolve boundary layers or initial layers in the transport solution. Section V is devoted to analyzing problems that are thick in certain frequency ranges, but thin or intermediate in others. In Section VI we test the predictions of the asymptotic analysis with a series of steady-state and transient test problems, some of which have extremely sharp boundary layers and some of which have wave fronts moving through the slab. We offer some concluding remarks in the final section.

II. ANALYSIS OF ANALYTIC SOLUTION

We consider the planar-geometry radiative transfer problem

$$\frac{\varepsilon}{c}\frac{\partial\psi}{\partial t}(x,\mu,\nu,t)+\mu\frac{\partial\psi}{\partial x}(x,\mu,\nu,t)+\frac{\sigma(x,\nu,T)}{\varepsilon}\psi(x,\mu,\nu,t)=\frac{\sigma(x,\nu,T)}{\varepsilon}B(\nu,T), \quad (1)$$

$$\varepsilon C_p(x,T)\frac{\partial T}{\partial t}=\int_0^\infty\int_{-1}^1\frac{\sigma(x,\nu,T)}{\varepsilon}[\psi(x,\mu,\nu,t)-B(\nu,T)]\,d\mu\,d\nu+\varepsilon Q(x,t), \quad (2)$$

$$\psi(0,\mu,\nu,t)=F(\mu,\nu,t), \qquad 0<\mu\le 1, \quad (3a)$$

$$\psi(X,\mu,\nu,t)=G(\mu,\nu,t), \qquad -1\le\mu<0, \quad (3b)$$

$$\psi(x,\mu,\nu,0)=\psi_i(x,\mu,\nu), \quad (4)$$

$$T(x,0)=T_i(x), \quad (5)$$

where B is the Planck function (integrated over the azimuthal direction, yielding a factor of 2π to which the reader may not be accustomed):

$$B(\nu,T)=\frac{4\pi h\nu^3}{c^2}\frac{1}{e^{h\nu/kT}-1}. \quad (6)$$

We also define the radiation energy density:

$$E_R(x,t)=aT_R^4(x,t)=\frac{1}{c}\int_0^\infty d\nu\int_{-1}^1 d\mu\psi(x,\mu,\nu,t). \quad (7)$$

If we set the parameter ε to unity, then Eqs. (1)–(5) constitute a radiative-transfer problem in standard notation: c is the speed of light, $\psi(x,\mu,\nu,t)$ is the specific intensity of particles at point x traveling in the "direction" μ at time t, $\sigma(x,\nu,T)$ is the opacity of the material at x at frequency ν given a material temperature $T(x,t)$, $Q(x,t)$ is the interior heat source, h is Planck's constant, k is Boltzmann's constant, and a is the radiation constant $(8\pi^5k^4)/(15h^3c^3)$.

If we take the functions ψ, σ, T, and B to be scaled such that they are $O(1)$, and let ε be a small parameter that tends toward zero, then Eqs. (1)–(5) are the starting point for an asymptotic analysis. The reader is encouraged to consult Refs. [1, 8] for justifications of this scaling and for details concerning the asymptotic analysis that we will now summarize specifically for slab geometry. Larsen *et al.* show [1] that away from boundaries, as $\varepsilon\to 0$

the leading-order analytic solution is Planckian,

$$\psi^{(0)}(x,\mu,\nu,t) = B\big(\nu, T^{(0)}(x,t)\big), \tag{8}$$

where the leading-order temperature $T^{(0)}$ satisfies the energy-balance equation

$$a\frac{\partial}{\partial t}\Big[\big(T^{(0)}\big)^4\Big] + C_p\big(x, T^{(0)}\big)\frac{\partial T^{(0)}}{\partial t} + \frac{\partial J^{(1)}}{\partial x} = Q(x,t), \tag{9}$$

where the $O(\varepsilon)$ "net flux" or "net current density" $J^{(1)}$ is

$$J^{(1)}(x) = -\frac{ac}{3\sigma_R\big(x, T^{(0)}\big)}\frac{\partial\big(T^{(0)}\big)^4}{\partial x}. \tag{10}$$

Here we have used the Rosseland mean opacity:

$$\frac{1}{\sigma_R(x,T)} \equiv \frac{\int_0^\infty \frac{1}{\sigma(x,\nu,T)}\frac{\partial B(\nu,T)}{\partial T}\,d\nu}{\int_0^\infty \frac{\partial B(\nu,T)}{\partial T}\,d\nu} = \frac{\int_0^\infty \frac{1}{\sigma(x,\nu,T)}\frac{\partial B(\nu,T)}{\partial T}\,d\nu}{4acT^3}. \tag{11}$$

We can combine Eqs. (9) and (10) to form a diffusion equation:

$$a\frac{\partial}{\partial t}\Big[\big(T^{(0)}\big)^4\Big] + C_p\big(x, T^{(0)}\big)\frac{\partial T^{(0)}}{\partial t} - \frac{\partial}{\partial x}\frac{ac}{3\sigma_R\big(x, T^{(0)}\big)}\frac{\partial\big(T^{(0)}\big)^4}{\partial x} = Q(x,t). \tag{12}$$

Pomraning [8] analyzes the "initial-layer" problem to find the initial condition for the leading-order temperature

$$a\big[T^{(0)}(x,0)\big]^4 + E\big(T^{(0)}(x,0)\big) = \frac{1}{c}\int_0^\infty d\nu\int_{-1}^1 d\mu\,\psi_i(x,\mu,\nu) + E(T_i(x)),$$

where E is the matter energy density. In our formulation of Eq. (2) we have assumed that $dE/dt = C_p(T)\,dT/dt$, which leads to

$$a\big[T^{(0)}(x,0)\big]^4 + \bar{C}_p(x)T^{(0)}(x,0) = \frac{1}{c}\int_0^\infty d\nu\int_{-1}^1 d\mu\,\psi_i(x,\mu,\nu) + \bar{C}_p(x)T_i(x), \tag{13}$$

where $\bar{C}_p(x)$ is an average over the interval $(T_i(x), T^{(0)}(x,0))$. Thus, the $T^{(0)}$ that satisfies this equation is the appropriate initial condition for our Eq. (12).

Pomraning also develops a half-space problem whose solution would yield the boundary condition satisfied by the leading-order temperature. This problem appears too difficult to solve analytically, but Pomraning uses a variational procedure to find an approximate solution. At the left boundary in our planar problem, for example, this yields

$T^{(0)}(x,t)|_{x=0} \approx T^{\text{var}}$, where

$$ac(T^{\text{var}})^4 = ac\big(T_M^{\text{ex}}\big)^4 + \sigma_R\big(0, T_M^{\text{ex}}\big)\int d\nu\int_0^1 d\mu 3\mu^2\frac{F(\nu,\mu,t) - B\big(\nu, T_M^{\text{ex}}\big)}{\sigma\big(0,\nu,T_M^{\text{ex}}\big)}, \tag{14a}$$

where we have defined the exact "Marshak" boundary temperature:

$$ac\left(T_M^{\text{ex}}\right)^4 = 2\int d\nu \int_0^1 d\mu 2\mu F(\nu, \mu, t). \tag{14b}$$

Similarly, at the right boundary Pomraning's result is

$T^{(0)}(x, t)|_{x=X} \approx T^{\text{var}}$, where

$$ac(T^{\text{var}})^4 = ac\left(T_M^{\text{ex}}\right)^4 + \sigma_R\left(X, T_M^{\text{ex}}\right)\int d\nu \int_{-1}^0 d\mu 3\mu^2 \frac{G(\nu, \mu, t) - B\left(\nu, T_M^{\text{ex}}\right)}{\sigma\left(X, \nu, T_M^{\text{ex}}\right)}, \tag{15a}$$

$$ac\left(T_M^{\text{ex}}\right)^4 = 2\int d\nu \int_{-1}^0 d\mu 2|\mu| G(\nu, \mu, t). \tag{15b}$$

We can rewrite Pomraning's boundary condition in a form that more closely resembles results from one-frequency-group diffusive problems. We define a Planckian-weighted inverse opacity:

$$\int d\nu \frac{B(\nu, T)}{\sigma(x, \nu, T)} = \frac{1}{\sigma_P(x, T)}\frac{1}{2}acT^4. \tag{16}$$

Then if we make liberal use of the definition (14b), it is possible to manipulate Eq. (14a) into the form

$$ac(T^{\text{var}})^4 = \int d\nu \int_0^1 d\mu \left[2\mu\left(2 - \frac{\sigma_R\left(0, T_M^{\text{ex}}\right)}{\sigma_P\left(0, T_M^{\text{ex}}\right)}\right) + 3\mu^2 \frac{\sigma_R\left(0, T_M^{\text{ex}}\right)}{\sigma\left(0, \nu, T_M^{\text{ex}}\right)}\right] F(\nu, \mu, t). \tag{17}$$

We note that given only one frequency group the opacity ratios become unity, and we have

$$ac\left(T_{1-\text{grp}}^{\text{var}}\right)^4 = \int_0^1 d\mu [2\mu + 3\mu^2] F(\mu, t). \tag{18}$$

(Similar results hold at the right boundary.) This is a variational approximation to the exact one-group boundary condition

$$ac\left(T_{1-\text{grp}}^{\text{var}}\right)^4 = \int_0^1 d\mu 2W(\mu) F(\mu, t), \tag{19}$$

where $W(\mu)$ is a known tabulated function ($\sqrt{3}\mu/2$ times Chandrasekhar's H-function), which has the approximations

$$W(\mu) = 0.91\mu + 1.635\mu^2 \pm \text{a few \%} \approx \mu + 3\mu^2/2. \tag{20}$$

To summarize, as $\varepsilon \to 0$, the leading-order part of the interior solution (valid away from the initial layer at $t = 0$ and boundary layers at $x = 0$ and $x = X$) is defined by Eq. (8), where the leading-order temperature satisfies Eqs. (12), with initial condition given by Eq. (13) and boundary conditions approximately given by Eqs. (14) and (15). Thus, the asymptotic interior transport solution satisfies a nonlinear one-group diffusion equation with known initial conditions and approximately known boundary conditions. In this paper we will show that the asymptotic solution of a *discretized* transport equation satisfies a robust discretization of this nonlinear diffusion equation, with boundary and initial conditions that are very good approximations to those described above.

III. THE "SIMPLE" CORNER-BALANCE METHOD

We now describe the simplest member of a family of subcell-balance methods developed recently for spatial discretization of the transport equation. This method was first described in a conference report [9] and generalized somewhat (for slab geometry) in a later summary [10]; more complete descriptions of it and a related method are found in Ref. [11].

We begin with a transport equation in *XY* geometry

$$\mu\frac{\partial\psi}{\partial x}+\eta\frac{\partial\psi}{\partial y}+\sigma(x,y)\psi(x,y,\vec{\Omega})=S(x,y,\vec{\Omega}),\qquad (x,y)\in D, \tag{21a}$$

$$\psi(x,y,\vec{\Omega})=F(x,y,\vec{\Omega}),\qquad (x,y)\in\partial D,\quad \vec{n}(x,y)\cdot\vec{\Omega}<0, \tag{21b}$$

where ∂D is the boundary of the spatial domain D and $\vec{n}$ is the outward unit normal. We divide the problem domain into polygonal cells and divide each cell into quadrilateral subcells that we call "corners," as shown in Fig. 1. The vectors appearing in Fig. 1 are edge lengths times outward unit normals for corner c. Corner c has two neighboring corners inside its polygonal cell, which we denote by c_1 (counterclockwise from c) and c_2 (clockwise). The corner has four bounding surfaces. Two surfaces are *inside* the cell: s_1 (adjacent to c_1) and s_2 (adjacent to c_2). The other two surfaces are on the cell boundary, and are denoted simply by "+" or "−" subscripts as shown.

We integrate the transport equation over corner c and use the divergence theorem to obtain a statement of conservation, or "balance," over the corner,

$$\vec{\Omega}\cdot\left[\vec{A}_{c+}\psi_{c+}(\vec{\Omega})+\vec{A}_{c-}\psi_{c-}(\vec{\Omega})+\vec{B}_{c+}\psi_{s_1}(\vec{\Omega})+\vec{B}_{c-}\psi_{s_2}(\vec{\Omega})\right]+\sigma_c V_c\psi_c(\vec{\Omega})=V_c S_c(\vec{\Omega}), \tag{22}$$

where V_c is the area of the corner and subscripts on functions denote averages: ψ_c is the average over corner c, ψ_{s_1} is the average over the surface s_1, etc. We use simple approximations to close the system

$$\psi_{s_1}=\left(\psi_c+\psi_{c_1}\right)/2, \tag{23a}$$

$$\psi_{s_2}=\left(\psi_c+\psi_{c_2}\right)/2, \tag{23b}$$

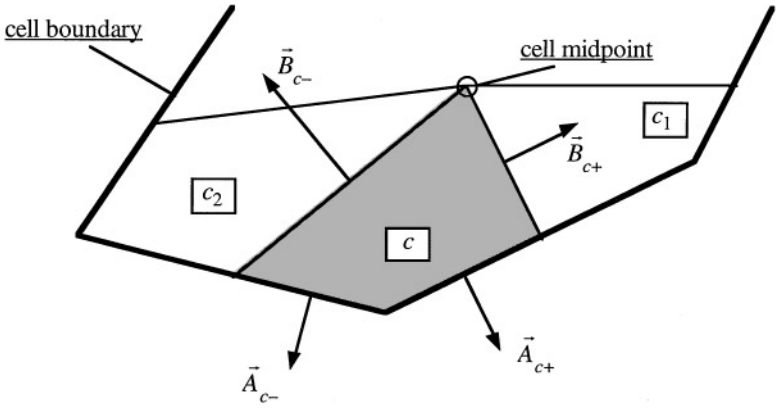

FIG. 1. A "corner" subcell, c, and its neighbors c_1 and c_2.

$$\psi_{c\pm} = \begin{cases} \psi_c, & \vec{A}_{c\pm} \cdot \vec{\Omega} > 0, \\ \psi_{inc,c\pm} \text{ (known)}, & \vec{A}_{c\pm} \cdot \vec{\Omega} < 0. \end{cases} \tag{23c}$$

This is SCB in its original form. As presented, the method has the following known properties [11]:

- Given rectangular cells, it is a robust and accurate method for one-group linear steady-state problems that are optically thick and diffusive.
- Given nonrectangular cells it gives reasonable solutions for thick, diffusive one-group linear steady-state problems, but its accuracy degrades as the grid distorts.
- Its accuracy is relatively poor away from the thick diffusive limit.

To overcome the latter problem, Eaton and Adams replaced Eq. (23c) in the one-dimensional SCB method with a more general equation, with very good results [10]. Adams took a different approach in Ref. [11] to overcome this and other problems in a 2D setting, again with good results. Both of the newer methods yield solutions that approach the SCB solution in the limit of thick diffusive spatial cells, at least in one-group steady-state settings. Because the newer methods behave similarly in the thick diffusive limit, the behavior of the SCB solution in that limit is of significant interest.

In the planar-geometry problem considered in this paper, SCB consists of two exact half-cell balance equations and two approximations per cell. The first approximation is that the cell-midpoint intensity equals the average,

$$\psi_j = (\psi_{jR} + \psi_{jL})/2, \tag{24}$$

and the second is that the exiting intensity from a cell equals the upstream half-cell average,

$$\psi_{j+1/2} = \begin{cases} \psi_{jR}, & 1 \le j \le N, \quad \mu > 0; \\ \psi_{j+1,L}, & 0 \le j \le N-1, \quad \mu < 0. \end{cases} \tag{25}$$

Here the subscript j refers to the jth cell and $j \pm 1/2$ to its edges. The subscripts jL/jR denote averages in the left/right halves of cell j, and μ is the x-component of the direction vector.

In the next section we apply SCB to the spatial variable in the radiative transfer equations, along with a finite-difference method for the time variable, the discrete-ordinates method for the direction variable, and a multigroup method for the frequency variable. We then perform an asymptotic analysis of this fully discrete problem.

IV. ASYMPTOTIC ANALYSIS OF THE DISCRETE PROBLEM

When we apply the discrete-ordinates (S_N) angular discretization, the multigroup discretization of frequency, and an (essentially) fully implicit (FI) time discretization to the scaled equations (1)–(2), we obtain

$$\frac{\varepsilon}{c}\frac{\psi_{mg}(x) - \psi_{mg}^k(x)}{\Delta t_k} + \mu_m \frac{d\psi_{mg}}{dx} + \frac{\sigma_g(x)}{\varepsilon}\psi_{mg}(x) = \frac{\sigma_g(x)}{\varepsilon} B_g(T), \tag{26}$$

$$\varepsilon C_p \frac{T(x) - T^k(x)}{\Delta t_k} = \sum_{g=1}^{G}\sum_{m=1}^{M} w_m \frac{\sigma_g(x)}{\varepsilon}[\psi_{mg}(x) - B_g(T(x))] + \varepsilon Q(x), \tag{27}$$

where μ is the x-component of the direction vector $\vec{\Omega}$, $\{(w_m, \mu_m), m = 1, \ldots, M\}$ is the

discrete-ordinates quadrature set, and g is the frequency-group subscript. Here the k superscript indicates the beginning of the time step (t_k, t_{k+1}), ψ and T without superscript are both time-step-averaged and end-of-step values, and Q is also averaged over the step. To avoid restricting the validity of this analysis we do not specify the definitions of the opacity and the specific heat in these equations. The opacity, for example, could be held explicit (i.e., evaluated at T^k), made fully implicit (evaluated at $T = T^{k+1}$), or anything in between (such as evaluated at an extrapolated temperature).

We now apply the SCB spatial discretization [10], described in the preceding section, to these equations. We assume a spatial grid of N cells, with cell edges defined by $x_{j\pm1/2}$, $j = 1, \ldots, N$. The subscripts jR and jL indicate left and right half-cell averages, respectively, in cell j. First we average Eqs. (26) and (27) over each half-cell:

$$\frac{\varepsilon}{c}\frac{\psi_{mg,jR} - \psi^k_{mg,jR}}{\Delta t_k} + \frac{\mu_m}{\Delta x_j/2}(\psi_{mg,j+1/2} - \psi_{mg,j}) + \frac{\sigma_{gjR}}{\varepsilon}\psi_{mg,jR} = \frac{\sigma_{gjR}}{\varepsilon}B_{g,jR}, \quad (28a)$$

$$\frac{\varepsilon}{c}\frac{\psi_{mg,jL} - \psi^k_{mg,jL}}{\Delta t_k} + \frac{\mu_m}{\Delta x_j/2}(\psi_{mg,j} - \psi_{mg,j-1/2}) + \frac{\sigma_{gjL}}{\varepsilon}\psi_{mg,jL} = \frac{\sigma_{gjL}}{\varepsilon}B_{g,jL}, \quad (28b)$$

$$\varepsilon C_{p,jH}\frac{T_{jH} - T^k_{jH}}{\Delta t_k} = \sum_{g=1}^{G}\sum_{m=1}^{M} w_m \frac{\sigma_{gjH}}{\varepsilon}[\psi_{mg,jH} - B_{g,jH}] + \varepsilon Q_{jH}, \qquad H = L \text{ or } R. \quad (29)$$

Next we impose our closure approximations:

$$\psi_{mg,j} = \frac{1}{2}(\psi_{mg,jR} + \psi_{mg,jL}), \quad (30a)$$

$$\psi_{mg,j+1/2} = \begin{cases} F_{mg} = F_g(\mu_m), & j = 0, \mu_m > 0; \\ \psi_{mg,jR}, & 1 \le j \le N, \mu_m > 0; \\ G_{mg} = G_g(\mu_m), & j = N, \mu_m < 0; \\ \psi_{mg,j+1,L}, & 0 \le j \le N-1, \mu_m < 0. \end{cases} \quad (30b)$$

Here the sources and boundary conditions are averages over the time step:

$$Q_{jH} \equiv \frac{1}{\Delta t_k}\int_{t_k}^{t_{k+1}} Q_H(t)\,dt, \qquad H = L \text{ or } R,$$
$$F_{mg} \equiv \frac{1}{\Delta t_k}\int_{t_k}^{t_{k+1}} F_{mg}(t)\,dt, \qquad G_{mg} \equiv \frac{1}{\Delta t_k}\int_{t_k}^{t_{k+1}} G_{mg}(t)\,dt. \quad (31)$$

Into these equations we introduce the expansions

$$\psi_{mgjH} = \psi^{(0)}_{mgjH} + \varepsilon\psi^{(1)}_{mgjH} + \varepsilon^2\psi^{(2)}_{mgjH} + \cdots, \quad (32a)$$

$$T_{jH} = T^{(0)}_{jH} + \varepsilon T^{(1)}_{jH} + \varepsilon^2 T^{(2)}_{jH} + \cdots, \quad (32b)$$

for each intensity and temperature that appears in the discrete system of equations. We introduce similar expansions for temperature-dependent quantities such as σ and B.

In what follows we shall often make use of the following notation:

$$[f_g]^{(k)} \equiv \text{coefficient of } \varepsilon^k \text{ in the product of the expansions of } f \text{ and } g.$$

Thus, for example, $[\sigma\psi]^{(1)}$ is a compact way to write $\sigma^{(0)}\psi^{(1)} + \sigma^{(1)}\psi^{(0)}$.

A. *Interior Analysis*

From the $O(1/\varepsilon)$ terms in Eqs. (28) we find that

$$\psi^{(0)}_{mg,jH} = B^{(0)}_{gjH} = B_g\left(T^{(0)}_{jH}\right), \qquad H = L \text{ or } R, \text{ all } j \text{ and } g, \tag{33}$$

where the $T^{(0)}_{jH}$ are as yet undetermined. This result, which states that the leading-order SCB intensities are isotropic and Planckian, is exactly like the analytic result, Eq. (8).

If we add Eq. (28a) for cell j to Eq. (28b) for cell $j+1$, consider the O(ε) terms, multiply by w_m, and sum over angles and groups, we obtain

$$\frac{a}{\Delta t_k}\left[\frac{\Delta x_j}{2}\left(\left(T^{(0)}_{jR}\right)^4 - \left(T^{(0)k}_{jR}\right)^4\right) + \frac{\Delta x_{j+1}}{2}\left(\left(T^{(0)}_{j+1,L}\right)^4 - \left(T^{(0)k}_{j+1,L}\right)^4\right)\right] + J^{(1)}_{j+1} - J^{(1)}_j$$
$$+ \sum_g \sum_m w_m \left\{\frac{\Delta x_j}{2}[\sigma(\psi_m - B)]^{(2)}_{gjR} + \frac{\Delta x_{j+1}}{2}[\sigma(\psi_m - B)]^{(2)}_{g,j+1,L}\right\} = 0,$$
$$j = 1, \ldots, N-1, \tag{34}$$

where the mid-cell "currents" (net fluxes) $J^{(1)}$ are defined:

$$J^{(1)}_j \equiv \sum_{g=1}^{G}\sum_{m=1}^{M} w_m \mu_m \psi^{(1)}_{mgj}. \tag{35}$$

In obtaining Eq. (34) we assumed that the leading-order intensity $\psi^{(0)k}$ at time t_k is Planckian at the temperature $T^{(0)k}$. For all but the first time step we know from Eq. (33) that this is true, so Eq. (34) certainly holds for $k > 0$. We must defer a precise statement about the initial time step ($k = 0$) until the initial-layer analysis in the next subsection.

We can simplify Eq. (34) somewhat by using the $O(\varepsilon)$ terms from Eq. (29), which are

$$\sum_g \sum_m w_m \frac{\Delta x_j}{2}[\sigma(\psi_m - B)]^{(2)}_{gjH} = \frac{\Delta x_j}{2} C^{(0)}_{p,jH} \frac{T^{(0)}_{jH} - T^{(0)k}_{jH}}{\Delta t_k} - \frac{\Delta x_j}{2} Q_{jH}. \tag{36}$$

Using this equality we can rewrite Eq. (34) as

$$\frac{a}{\Delta t_k}\left[\frac{\Delta x_j}{2}\left(\left(T^{(0)}_{jR}\right)^4 - \left(T^{(0)k}_{jR}\right)^4\right) + \frac{\Delta x_{j+1}}{2}\left(\left(T^{(0)}_{j+1,L}\right)^4 - \left(T^{(0)k}_{j+1,L}\right)^4\right)\right]$$
$$+ \frac{1}{\Delta t_k}\left[\frac{\Delta x_j}{2} C^{(0)}_{p,jR}\left(T^{(0)}_{jR} - T^{(0)k}_{jR}\right) + \frac{\Delta x_{j+1}}{2} C^{(0)}_{p,j+1,L}\left(T^{(0)}_{j+1,L} - T^{(0)k}_{j+1,L}\right)\right]$$
$$+ J^{(1)}_{j+1} - J^{(1)}_j = \frac{\Delta x_j}{2} Q_{jR} + \frac{\Delta x_{j+1}}{2} Q_{j+1,L}, \qquad j = 1, \ldots, N-1. \tag{37}$$

We recognize that this is simply the spatial integral from x_j to x_{j+1} and time integral from t_k to t_{k+1} of the analytic leading-order energy balance equation (9), at least if the specific heats, opacities, and net fluxes are appropriately time averaged. Thus, this equation is essentially exact.

The next part of this analysis will show that the leading-order temperatures are continuous, that is, that $T^{(0)}_{jR} = T^{(0)}_{j+1,L}$. It will also find the leading-order temperatures in the boundary

half-cells, $T_{1L}^{(0)}$ and $T_{NR}^{(0)}$. We begin with the $O(1)$ terms of Eqs. (28) and (29):

$$\frac{\mu_m}{\Delta x_j/2}\left(\psi_{mg,j+1/2}^{(0)} - \psi_{mg,j}^{(0)}\right) + [\sigma(\psi_m - B)]_{gjR}^{(1)} = 0, \tag{38a}$$

$$\frac{\mu_m}{\Delta x_j/2}\left(\psi_{mg,j}^{(0)} - \psi_{mg,j-1/2}^{(0)}\right) + [\sigma(\psi_m - B)]_{gjL}^{(1)} = 0 \tag{38b}$$

$$0 = \sum_{g=1}^{G}\sum_{m=1}^{M} w_m [\sigma(\psi_m - B)]_{gjH}^{(1)}, \qquad H = L \text{ or } R. \tag{39}$$

If we multiply Eqs. (38) by w_m and sum over m and g we obtain

$$\frac{1}{\Delta x_j/2}\sum_{g=1}^{G}\sum_{m=1}^{M} w_m\mu_m\left(\psi_{mg,j+1/2}^{(0)} - \psi_{mg,j}^{(0)}\right) + \sum_{g=1}^{G}\sum_{m=1}^{M} w_m [\sigma(\psi_m - B)]_{gjR}^{(1)} = 0, \tag{40a}$$

$$\frac{1}{\Delta x_j/2}\sum_{g=1}^{G}\sum_{m=1}^{M} w_m\mu_m\left(\psi_{mg,j}^{(0)} - \psi_{mg,j-1/2}^{(0)}\right) + \sum_{g=1}^{G}\sum_{m=1}^{M} w_m [\sigma(\psi_m - B)]_{gjL}^{(1)} = 0. \tag{40b}$$

We see from Eq. (33) that $\psi_{mg,j}^{(0)}$ is isotropic; thus, provided the quadrature set correctly integrates μ to zero, the $\psi_{mg,j}^{(0)}$ terms in Eqs. (40) vanish. We shall henceforth *assume a symmetric quadrature set*, which does correctly integrate μ to zero. We see from Eq. (39) that the last double summation in each of Eqs. (15) is zero, and we are left with

$$\sum_{g=1}^{G}\sum_{m=1}^{M} w_m\mu_m\psi_{mg,j+1/2}^{(0)} = 0, \qquad j = 0, \ldots, N,$$

which says that to leading order, the cell-edge net fluxes are zero. We can rewrite this as

$$\sum_{g=1}^{G}\sum_{\mu_m>0} w_m\mu_m\psi_{mg,j+1/2}^{(0)} = \sum_{g=1}^{G}\sum_{\mu_m<0} w_m|\mu_m|\psi_{mg,j+1/2}^{(0)}, \qquad j = 0, \ldots, N. \tag{41}$$

If we consider interior cell edges, which means $j = 1, \ldots, N-1$, then by the definition (30b) of the cell-edge angular fluxes we have

$$\sum_{g=1}^{G}\sum_{\mu_m>0} w_m\mu_m\psi_{mg,jR}^{(0)} = \sum_{g=1}^{G}\sum_{\mu_m<0} w_m|\mu_m|\psi_{mg,j+1,L}^{(0)}, \qquad j = 1, \ldots, N-1.$$

Now we use the result (33) that the leading-order angular fluxes are isotropic and Planckian, and we find

$$\sum_{g} B_{gjR}^{(0)}\left(\sum_{\mu_m>0} w_m\mu_m\right) = \sum_{g} B_{g,j+1,L}^{(0)}\left(\sum_{\mu_m<0} w_m|\mu_m|\right), \qquad j = 1, \ldots, N-1.$$

Because we have assumed a symmetric quadrature set and B_g sums to $acT^4/2$, this result implies that the leading-order temperature is continuous across cell interfaces:

$$T_{jR}^{(0)} = T_{j+1,L}^{(0)} \equiv T_{j+1/2}^{(0)}, \qquad j = 1, \ldots, N-1. \tag{42}$$

It follows that $B_g^{(0)}$ and $\psi_g^{(0)}$ are also continuous across interior cell interfaces

$$B_{gjR}^{(0)} = B_{g,j+1,L}^{(0)} \equiv B_{g,j+1/2}^{(0)}, \qquad \psi_{mgjR}^{(0)} = \psi_{mg,j+1,L}^{(0)} \equiv \psi_{mg,j+1/2}^{(0)}, \quad j = 1, \ldots, N-1. \tag{43}$$

We must also consider Eq. (41) at the problem boundaries. At the left boundary we have

$$\sum_g \sum_{\mu_m>0} w_m \mu_m F_{mg} = \sum_g \sum_{\mu_m<0} w_m |\mu_m| B_{g,1L}^{(0)},$$

or

$$ac\left[T_{1L}^{(0)}\right]^4 \equiv acT_{M,1/2}^4 = 2\sum_g \sum_{\mu_m>0} w_m \frac{2\mu_m}{\rho} F_{mg}, \qquad \rho \equiv 2\sum_{\mu_m>0} w_m \mu_m \approx 1. \tag{44a}$$

We have used the subscript M to denote that this is a "Marshak" boundary-condition temperature, the discrete-ordinates and multigroup approximation to Eq. (14b). A similar result holds on the right:

$$ac\left[T_{NR}^{(0)}\right]^4 \equiv acT_{M,N+1/2}^4 = 2\sum_g \sum_{\mu_m<0} w_m \frac{2|\mu_m|}{\rho} G_{mg}. \tag{44b}$$

Although these are the leading-order temperatures obtained by the SCB method in the boundary half-cells, we shall see later that these are *not* the boundary temperatures that govern the interior SCB solution.

The remainder of the interior analysis is devoted to obtaining expressions for $J^{(1)}$ in terms of $T^{(0)}$. We return to the $O(1)$ equations (38), each of which we divide by a leading-order opacity:

$$\frac{\mu_m}{\sigma_{gjR}^{(0)} \Delta x_j/2}\left(\psi_{mg,j+1/2}^{(0)} - \psi_{mg,j}^{(0)}\right) + [\psi_m - B]_{gjR}^{(1)} + \frac{\sigma_{gjR}^{(1)}}{\sigma_{gjR}^{(0)}}[\psi_m - B]_{gjR}^{(0)} = 0, \tag{45a}$$

$$\frac{\mu_m}{\sigma_{gjL}^{(0)} \Delta x_j/2}\left(\psi_{mg,j}^{(0)} - \psi_{mg,j-1/2}^{(0)}\right) + [\psi_m - B]_{gjL}^{(1)} + \frac{\sigma_{gjL}^{(1)}}{\sigma_{gjL}^{(0)}}[\psi_m - B]_{gjL}^{(0)} = 0. \tag{45b}$$

We recognize from Eq. (33) that the last term in each equation vanishes. We multiply by $w_m \mu_m$, sum over m and g, and rearrange to obtain

$$\sum_{g=1}^{G}\sum_{m=1}^{M} w_m \mu_m \psi_{mg,jR}^{(1)} = -\frac{1}{\sigma_{gjR}^{(0)} \Delta x_j/2}\sum_{g=1}^{G}\sum_{m=1}^{M} w_m \mu_m^2 \left(\psi_{mg,j+1/2}^{(0)} - \psi_{mg,j}^{(0)}\right), \tag{46a}$$

$$\sum_{g=1}^{G}\sum_{m=1}^{M} w_m \mu_m \psi_{mg,jL}^{(1)} = -\frac{1}{\sigma_{gjL}^{(0)} \Delta x_j/2}\sum_{g=1}^{G}\sum_{m=1}^{M} w_m \mu_m^2 \left(\psi_{mg,j}^{(0)} - \psi_{mg,j-1/2}^{(0)}\right). \tag{46b}$$

Upon adding these equations and dividing by two we obtain the desired relation between the net currents $J^{(1)}$ and the leading-order intensities:

$$J_j^{(1)} = -\sum_{g=1}^{G}\sum_{m=1}^{M} w_m \mu_m^2 \left(\frac{\psi_{mg,j+1/2}^{(0)} - \psi_{mg,j}^{(0)}}{\sigma_{gjR}^{(0)} \Delta x_j} + \frac{\psi_{mg,j}^{(0)} - \psi_{mg,j-1/2}^{(0)}}{\sigma_{gjL}^{(0)} \Delta x_j}\right). \tag{47}$$

This expression requires some manipulation before it serves our purposes. Let us first consider interior cells, for which $\psi^{(0)}_{mgj}$ is the average of $\psi^{(0)}_{mgj\pm1/2}$ [by Eqs. (33) and Eq. (43)]. Then our expression simplifies to

$$J^{(1)}_j = -\sum_{g=1}^{G}\sum_m w_m\mu_m^2\left(\frac{\psi^{(0)}_{mg,j+1/2}-\psi^{(0)}_{mg,j-1/2}}{\Delta x_j}\right)\frac{1}{2}\left(\frac{1}{\sigma^{(0)}_{gjR}}+\frac{1}{\sigma^{(0)}_{gjL}}\right), \qquad j=2,\ldots,N-1.$$

We define a cell-averaged opacity

$$\frac{1}{\sigma^{(0)}_{gj}} \equiv \frac{1}{2}\left(\frac{1}{\sigma^{(0)}_{gjR}}+\frac{1}{\sigma^{(0)}_{jgL}}\right) \tag{48}$$

and recall that the leading-order intensities are isotropic and Planckian; then we have

$$J^{(1)}_j = -\sum_{g=1}^{G}\left(\frac{2B_g\big(T^{(0)}_{j+1/2}\big)-2B_g\big(T^{(0)}_{j-1/2}\big)}{3\sigma^{(0)}_{gj}\Delta x_j}\right), \qquad j=2,\ldots,N-1, \tag{49a}$$

or

$$J^{(1)}_j = -\frac{ac}{3\big\langle\sigma^{(0)}_{gj}\big\rangle}\frac{\big(T^{(0)}_{j+1/2}\big)^4-\big(T^{(0)}_{j-1/2}\big)^4}{\Delta x_j}, \qquad j=2,\ldots,N-1, \tag{49b}$$

where $\langle\sigma\rangle$ is an approximate cell-averaged Rosseland mean:

$$\frac{1}{\big\langle\sigma^{(0)}_j\big\rangle} = \sum_{g=1}^{G}\left\{\frac{1}{\sigma^{(0)}_{gj}}\left(\frac{B_g\big(T^{(0)}_{j+1/2}\big)-B_g\big(T^{(0)}_{j-1/2}\big)}{T^{(0)}_{j+1/2}-T^{(0)}_{j-1/2}}\right)\right\}\Bigg/\sum_{g=1}^{G}\left(\frac{B_g\big(T^{(0)}_{j+1/2}\big)-B_g\big(T^{(0)}_{j-1/2}\big)}{T^{(0)}_{j+1/2}-T^{(0)}_{j-1/2}}\right). \tag{50}$$

(We have assumed here that the quadrature set correctly integrates μ^2 to $2/3$.) This is a reasonable discretization of the analytic expression (10). Considering this equation and the conservation equation (37), we see that *the leading-order discrete solution satisfies a reasonable discretization of the equilibrium diffusion equation*, at least in the interior of the slab after the initial time step.

B. *Initial-Layer Analysis*

Here we examine the first time step ($k=0$), for which the analog of Eq. (37) is

$$\begin{aligned}
&\frac{a}{\Delta t_k}\left[\frac{\Delta x_j}{2}\left(\big(T^{(0)}_{jR}\big)^4-\frac{1}{ac}\sum_{g=1}^{G}\sum_{m=1}^{M}w_m\psi_{i,mgjR}\right)\right.\\
&\quad\left.+\frac{\Delta x_{j+1}}{2}\left(\big(T^{(0)}_{j+1,L}\big)^4-\frac{1}{ac}\sum_{g=1}^{G}\sum_{m=1}^{M}w_m\psi_{i,mg,j+1,L}\right)\right]\\
&\quad+\frac{1}{\Delta t_k}\left[\frac{\Delta x_j}{2}C^{(0)}_{p,jR}\big(T^{(0)}_{jR}-T_{i,jR}\big)+\frac{\Delta x_{j+1}}{2}C^{(0)}_{p,j+1,L}\big(T^{(0)}_{j+1,L}-T_{i,j+1,L}\big)\right]\\
&\quad+J^{(1)}_{j+1}-J^{(1)}_j=\frac{\Delta x_j}{2}Q_{jR}+\frac{\Delta x_{j+1}}{2}Q_{j+1,L}, \qquad j=1,\ldots,N-1.
\end{aligned} \tag{51}$$

If the initial intensity in each half-cell is a Planckian at the initial temperature of the half-cell,

then the double summations in this equation become acT_i^4, and we have Eq. (37) again, with $T^{(0)k}|_{k=0} = T_i$. In the more general case we must find an initial temperature, $T^{(0)k}|_{k=0}$, in each half-cell, such that Eq. (51) is equivalent to Eq. (37) with $k = 0$. It is clear that this will be true for $T^{(0)k}|_{k=0}$ satisfying

$$\left\{a\left(T_{jH}^{(0)k}\right)^4 + C_{p,jH}^{(0)} T_{jH}^{(0)k}\right\}_{k=0} = \frac{1}{c}\sum_{g=1}^{G}\sum_{m=1}^{M} w_m \psi_{i,mgjH} + C_{p,jH}^{(0)} T_{i,jH}, \qquad H = L \text{ or } R. \tag{52}$$

Thus, Eq. (52) defines the initial condition for Eq. (37). Equation (52) is a very good approximation of Eq. (13), which defines the *exact* initial condition:

$$a\left[T^{(0)}(x,0)\right]^4 + \overline{C_p}(x)T^{(0)}(x,0) = \frac{1}{c}\int_0^\infty d\nu \int_{-1}^{1} d\mu \psi_i(x,\mu,\nu) + \overline{C_p}(x)T_i(x).$$

The only differences between the initial conditions for the discrete and exact equations are as follows:

- The integrals in the exact condition are replaced by summations in the discrete condition. Thus, the quadrature set and group structure should be chosen such that they accurately integrate the initial intensity.
- The C_p in the exact condition is an average over the temperature interval (T_i(x), $T^{(0)}$(x, 0)), whereas the C_p in the discrete condition is determined by the details of the time-differencing algorithm. This suggests that for greatest accuracy the time-differencing algorithm should use an average C_p over each time interval (as opposed, for example, to using C_p evaluated at the beginning-of-step temperature).

We conclude that the initial condition for the discretized conservation equation (37) is very accurate in most cases.

C. *Boundary-Layer Analysis*

The final part of the analysis is to explore what happens at boundaries, where there can be boundary layers that are not resolved by the spatial mesh. We consider first the cell at the left boundary, $j = 1$, for which we must simplify Eq. (47). We note that

$$\begin{aligned}\psi_{mg,3/2}^{(0)} - \psi_{mg,1}^{(0)} &= B_g\left(T_{3/2}^{(0)}\right) - \frac{1}{2}\left(B_g\left(T_{3/2}^{(0)}\right) + B_g(T_{M,1/2})\right) \\ &= \frac{1}{2}\left(B_g\left(T_{3/2}^{(0)}\right) - B_g(T_{M,1/2})\right) \qquad (53a)\end{aligned}$$

$$\psi_{mg,1}^{(0)} - \psi_{mg,1/2}^{(0)} = \frac{1}{2}\left(B_g\left(T_{3/2}^{(0)}\right) + B_g(T_{M,1/2}) - 2\psi_{mg,1/2}^{(0)}\right). \qquad (53b)$$

Using these identities we rewrite Eq. (47) for $j = 1$:

$$J_1^{(1)} = -\sum_{g=1}^{G}\sum_{m=1}^{M} w_m \mu_m^2 \left(\frac{B_g\left(T_{3/2}^{(0)}\right) - B_g(T_{M,1/2})}{2\sigma_{g1R}^{(0)}\Delta x_1} + \frac{B_g\left(T_{3/2}^{(0)}\right) + B_g(T_{M,1/2}) - 2\psi_{mg,1/2}^{(0)}}{2\sigma_{g1L}^{(0)}\Delta x_1}\right). \tag{54}$$

We require this expression to have the same form as Eq. (49a), the expression for the net current density in interior cells, for some value of $T_{1/2}^{(0)}$ that is yet undefined. That is, we

require that

$$\sum_{g=1}^{G}\left(\frac{2B_g\left(T_{3/2}^{(0)}\right)-2B_g\left(T_{1/2}^{(0)}\right)}{3\sigma_{g1}^{(0)}\Delta x_1}\right)$$
$$=\sum_{g=1}^{G}\sum_{m=1}^{M}w_m\mu_m^2\left(\frac{B_g\left(T_{3/2}^{(0)}\right)-B_g(T_{M,1/2})}{2\sigma_{g1R}^{(0)}\Delta x_1}+\frac{B_g\left(T_{3/2}^{(0)}\right)+B_g(T_{M,1/2})-2\psi_{mg,1/2}^{(0)}}{2\sigma_{g1L}^{(0)}\Delta x_1}\right). \tag{55}$$

We must find $T_{1/2}^{(0)}$ such that this is true. This will be the boundary condition of the discrete interior solution. We note first that the terms involving $T_{3/2}^{(0)}$ cancel out of the equation [recall the definition (48)], which leaves

$$\sum_{g=1}^{G}\left(\frac{2B_g\left(T_{1/2}^{(0)}\right)}{3\sigma_{g1}^{(0)}}\right)=\sum_{g=1}^{G}\sum_{m=1}^{M}w_m\mu_m^2\left(\frac{B_g(T_{M,1/2})}{2\sigma_{g1R}^{(0)}}-\frac{B_g(T_{M,1/2})-2\psi_{mg,1/2}^{(0)}}{2\sigma_{g1L}^{(0)}}\right). \tag{56}$$

To obtain an expression for $T_{1/2}^{(0)}$ we must perform some algebra:

$$\sum_{g=1}^{G}\left(\frac{B_g\left(T_{1/2}^{(0)}\right)}{\sigma_{g1}^{(0)}}\right)=\sum_{g=1}^{G}\sum_{m=1}^{M}w_m\frac{3}{2}\mu_m^2\left(B_g(T_{M,1/2})\left[\frac{1}{2\sigma_{g1R}^{(0)}}+\frac{1}{2\sigma_{g1L}^{(0)}}-\frac{1}{\sigma_{g1L}^{(0)}}\right]+\frac{\psi_{mg,1/2}^{(0)}}{\sigma_{g1L}^{(0)}}\right),$$
$$\Rightarrow\sum_{g=1}^{G}\left(\frac{B_g\left(T_{1/2}^{(0)}\right)}{\sigma_{g1}^{(0)}}\right)=\sum_{g=1}^{G}B_g(T_{M,1/2})\left[\frac{1}{\sigma_{g1}^{(0)}}-\frac{1}{\sigma_{g1L}^{(0)}}\right]+\sum_{g=1}^{G}\sum_{m=1}^{M}w_m\frac{3}{2}\mu_m^2\frac{\psi_{mg,1/2}^{(0)}}{\sigma_{g1L}^{(0)}},$$
$$\Rightarrow\sum_{g=1}^{G}\left(\frac{B_g\left(T_{1/2}^{(0)}\right)-B_g(T_{M,1/2})}{\sigma_{g1}^{(0)}}\right)=\sum_{g=1}^{G}B_g(T_{M,1/2})\left[-\frac{1}{\sigma_{g1L}^{(0)}}\right]$$
$$+\sum_{g=1}^{G}\sum_{\mu_m>0}w_m\frac{3}{2}\mu_m^2\frac{F_{mg}}{\sigma_{g1L}^{(0)}}+\sum_{g=1}^{G}\sum_{\mu_m<0}w_m\frac{3}{2}\mu_m^2\frac{B_g(T_{M,1/2})}{\sigma_{g1L}^{(0)}},$$

or

$$\sum_{g=1}^{G}\left(\frac{B_g\left(T_{1/2}^{(0)}\right)-B_g(T_{M,1/2})}{\sigma_{g1}^{(0)}}\right)=\sum_{g=1}^{G}\sum_{\mu_m>0}w_m\frac{3}{2}\mu_m^2\frac{F_{mg}-B_g(T_{M,1/2})}{\sigma_{g1L}^{(0)}}. \tag{57}$$

We now define an approximate Rosseland mean opacity evaluated at an average *boundary-layer* temperature:

$$\frac{1}{\left\langle\sigma_{1/2}^{(0)}\right\rangle}\equiv\sum_{g=1}^{G}\frac{1}{\sigma_{g1}^{(0)}}\left[\frac{B_g\left(T_{1/2}^{(0)}\right)-B_g(T_{M,1/2})}{T_{1/2}^{(0)}-T_{M,1/2}}\right]\Bigg/\sum_{g=1}^{G}\left[\frac{B_g\left(T_{1/2}^{(0)}\right)-B_g(T_{M,1/2})}{T_{1/2}^{(0)}-T_{M,1/2}}\right]. \tag{58}$$

We use this to rewrite Eq. (57):

$$\frac{1}{\left\langle\sigma_{1/2}^{(0)}\right\rangle}\frac{ac}{2}\left[\left(T_{1/2}^{(0)}\right)^4-(T_{M,1/2})^4\right]=\sum_{g=1}^{G}\sum_{\mu_m>0}w_m\frac{3}{2}\mu_m^2\frac{F_{mg}-B_g(T_{M,1/2})}{\sigma_{g1L}^{(0)}},$$

or

$$ac\left(T_{1/2}^{(0)}\right)^4 = ac(T_{M,1/2})^4 + \left\langle\sigma_{1/2}^{(0)}\right\rangle \sum_{g=1}^{G} \sum_{\mu_m>0} w_m 3\mu_m^2 \frac{F_{mg} - B_g(T_{M,1/2})}{\sigma_{g1L}^{(0)}}. \tag{59}$$

We define a Planckian-weighted inverse opacity,

$$\sum_{g=1}^{G} \frac{B_g(T_{M,1/2})}{\sigma_{g,1L}^{(0)}} = \frac{1}{\sigma_{P,1L}^{(0)}} \frac{1}{2} ac T_{M,1/2}^4, \tag{60}$$

which allows us to rewrite the boundary condition:

$$ac\left(T_{1/2}^{(0)}\right)^4 = \sum_{g=1}^{G} \sum_{\mu_m>0} w_m \left[\frac{2\mu}{\rho}\left(2 - \frac{\left\langle\sigma_{1/2}^{(0)}\right\rangle}{\sigma_{P,1L}^{(0)}}\right) + 3\mu_m^2 \frac{\left\langle\sigma_{1/2}^{(0)}\right\rangle}{\sigma_{g1L}^{(0)}}\right] F_{mg}. \tag{61a}$$

A similar result holds at the right boundary,

$$ac\left(T_{N+1/2}^{(0)}\right)^4 = \sum_{g=1}^{G} \sum_{\mu_m<0} w_m \left[\frac{2|\mu|}{\rho}\left(2 - \frac{\left\langle\sigma_{N+1/2}^{(0)}\right\rangle}{\sigma_{P,NR}^{(0)}}\right) + 3\mu_m^2 \frac{\left\langle\sigma_{N+1/2}^{(0)}\right\rangle}{\sigma_{gNR}^{(0)}}\right] G_{mg}, \tag{61b}$$

where

$$\frac{1}{\left\langle\sigma_{N+1/2}^{(0)}\right\rangle} \equiv \sum_{g=1}^{G} \frac{1}{\sigma_{gN}^{(0)}} \left[\frac{B_g\left(T_{N+1/2}^{(0)}\right) - B_g(T_{M,N+1/2})}{T_{N+1/2}^{(0)} - T_{M,N+1/2}}\right] \Bigg/ \sum_{g=1}^{G} \left[\frac{B_g\left(T_{N+1/2}^{(0)}\right) - B_g(T_{M,N+1/2})}{T_{N+1/2}^{(0)} - T_{M,N+1/2}}\right], \tag{62a}$$

$$\sum_{g=1}^{G} \frac{B_g(T_{M,N+1/2})}{\sigma_{g,NR}^{(0)}} = \frac{1}{\sigma_{P,NR}^{(0)}} \frac{1}{2} ac T_{M,N+1/2}^4. \tag{62b}$$

Equations (61) define the boundary conditions satisfied by the leading-order SCB solution in the interior of the slab. With these definitions, Eq. (49b) now holds for all j:

$$J_j^{(1)} = -\frac{ac}{3\left\langle\sigma_j^{(0)}\right\rangle} \frac{\left(T_{j+1/2}^{(0)}\right)^4 - \left(T_{j-1/2}^{(0)}\right)^4}{\Delta x_j}, \qquad j = 1, \ldots, N. \tag{63}$$

If we insert this into the balance equation (37) and note the continuity result (42), we obtain a reasonable discretization of the equilibrium diffusion equation (12):

$$\begin{aligned}
&\frac{a}{\Delta t_k} \frac{\Delta x_j + \Delta x_{j+1}}{2} \left[\left(T_{j+1/2}^{(0)}\right)^4 - \left(T_{j+1/2}^{(0)k}\right)^4\right] \\
&\quad + \frac{1}{\Delta t_k} \frac{C_{pjR}^{(0)} \Delta x_j + C_{p,j+1,L}^{(0)} \Delta x_{j+1}}{2} \left[T_{j+1/2}^{(0)} - T_{j+1/2}^{(0)k}\right] \\
&\quad - \frac{ac}{3\langle\sigma_{j+1}\rangle \Delta x_{j+1}} \left[\left(T_{j+3/2}^{(0)}\right)^4 - \left(T_{j+1/2}^{(0)}\right)^4\right] + \frac{ac}{3\langle\sigma_j\rangle \Delta x_j} \left[\left(T_{j+1/2}^{(0)}\right)^4 - \left(T_{j-1/2}^{(0)}\right)^4\right] \\
&= \frac{\Delta x_j}{2} Q_{jR} + \frac{\Delta x_{j+1}}{2} Q_{j+1}, L, \qquad j = 1, \ldots, N-1.
\end{aligned} \tag{64}$$

Here the boundary values $T_{1/2}$ and $T_{N+1/2}$ are given by Eqs. (61). Initial values T^k for $k = 0$ are given by Eq. (52).

D. *Comparison of Boundary Conditions*

We now compare the boundary conditions from the SCB and LLD methods against each other and against the variational result obtained by Pomraning. At the left boundary the three conditions are

$$\text{SCB:}\quad ac\left(T_{1/2}^{(0)}\right)^4\Big|_{\text{SCB}} = \sum_{g=1}^{G}\sum_{\mu_m>0} w_m\left[\frac{2\mu_m}{\rho}(2-r_{\text{SCB}}) + 3\mu_m^2 q_{g,\text{SCB}}\right]F_{mg}, \tag{65a}$$

$$\text{LLD:}\quad ac\left(T_{1/2}^{(0)}\right)^4\Big|_{\text{LLD}} = \sum_{g=1}^{G}\sum_{\mu_m>0} w_m\left[\frac{2\mu_m}{\rho}(2-r_{\text{LLD}}) + 3\mu_m^2 q_{g,\text{LLD}}\right]F_{mg}, \tag{65b}$$

$$\text{VAR:}\quad ac(T^{\text{var}})^4 = \int d\nu \int_0^1 d\mu\left[2\mu(2-r_{\text{var}}) + 3\mu^2 q_{g,\text{var}}\right]F(\nu,\mu,t), \tag{65c}$$

where the opacity ratios r and q are

$$r_{\text{SCB}} = \frac{\left\langle\sigma_{1/2}^{(0)}\right\rangle}{\sigma_{P,1L}} = \frac{\sum_{g=1}^{G}\frac{B_g(T_{M,1/2})}{\sigma_g(T_{M,1/2})}}{\sum_{g=1}^{G}B_g(T_{M,1/2})}\frac{\sum_{g=1}^{G}\left[\frac{B_g\left(T_{1/2}^{(0)}\right)-B_g(T_{M,1/2})}{T_{1/2}^{(0)}-T_{M,1/2}}\right]}{\sum_{g=1}^{G}\left[\frac{1}{2}\left(\frac{1}{\sigma_g(T_{M,1/2})}+\frac{1}{\sigma_g\left(T_{3/2}^{(0)}\right)}\right)\right]\left[\frac{B_g\left(T_{1/2}^{(0)}\right)-B_g(T_{M,1/2})}{T_{1/2}^{(0)}-T_{M,1/2}}\right]}, \tag{66a}$$

$$r_{\text{LLD}} = \frac{\left\langle\sigma_{1/2}^{(0)}\right\rangle_{\text{LLD}}}{\sigma_{P,1}} = \frac{\sum_{g=1}^{G}\frac{B_g(T_{M,1/2})}{\sigma_g\left(\frac{T_{M,1/2}+T_{3/2}^{(0)}}{2}\right)}}{\sum_{g=1}^{G}B_g(T_{M,1/2})}\frac{\sum_{g=1}^{G}\left[\frac{B_g\left(T_{1/2}^{(0)}\right)-B_g(T_{M,1/2})}{T_{1/2}^{(0)}-T_{M,1/2}}\right]}{\sum_{g=1}^{G}\frac{1}{\sigma_g\left(\frac{T_{M,1/2}+T_{3/2}^{(0)}}{2}\right)}\left[\frac{B_g\left(T_{1/2}^{(0)}\right)-B_g(T_{M,1/2})}{T_{1/2}^{(0)}-T_{M,1/2}}\right]}, \tag{66b}$$

$$r_{\text{var}} = \frac{\sigma_R\left(0,T_M^{\text{ex}}\right)}{\sigma_P\left(0,T_M^{\text{ex}}\right)} = \frac{\int\frac{B\left(\nu,T_M^{\text{ex}}\right)}{\sigma\left(\nu,T_M^{\text{ex}}\right)}d\nu}{\int B\left(\nu,T_M^{\text{ex}}\right)d\nu}\frac{\int\frac{\partial B\left(\nu,T_M^{\text{ex}}\right)}{\partial T}d\nu}{\int\frac{1}{\sigma\left(\nu,T_M^{\text{ex}}\right)}\frac{\partial B\left(\nu,T_M^{\text{ex}}\right)}{\partial T}d\nu}, \tag{66c}$$

$$q_{g,\text{SCB}} = \frac{\left\langle\sigma_{1/2}^{(0)}\right\rangle}{\sigma_{g1L}^{(0)}} = \frac{\frac{1}{\sigma_g(T_{M,1/2})}\sum_{g=1}^{G}\left[\frac{B_g\left(T_{1/2}^{(0)}\right)-B_g(T_{M,1/2})}{T_{1/2}^{(0)}-T_{M,1/2}}\right]}{\sum_{g=1}^{G}\left[\frac{1}{2}\left(\frac{1}{\sigma_g(T_{M,1/2})}+\frac{1}{\sigma_g\left(T_{3/2}^{(0)}\right)}\right)\right]\left[\frac{B_g\left(T_{1/2}^{(0)}\right)-B_g(T_{M,1/2})}{T_{1/2}^{(0)}-T_{M,1/2}}\right]}, \tag{67a}$$

$$q_{g,\text{LLD}} = \frac{\left\langle\sigma_{1/2}^{(0)}\right\rangle_{\text{LLD}}}{\sigma_{g1}^{(0)}} = \frac{\frac{1}{\sigma_g\left(\frac{T_{M,1/2}+T_{3/2}^{(0)}}{2}\right)}\sum_{g=1}^{G}\left[\frac{B_g\left(T_{1/2}^{(0)}\right)-B_g(T_{M,1/2})}{T_{1/2}^{(0)}-T_{M,1/2}}\right]}{\sum_{g=1}^{G}\frac{1}{\sigma_g\left(\frac{T_{M,1/2}+T_{3/2}^{(0)}}{2}\right)}\left[\frac{B_g\left(T_{1/2}^{(0)}\right)-B_g(T_{M,1/2})}{T_{1/2}^{(0)}-T_{M,1/2}}\right]}, \tag{67b}$$

$$q_{\text{var}}(\nu) = \frac{\sigma_R\left(0,T_M^{\text{ex}}\right)}{\sigma\left(0,\nu,T_M^{\text{ex}}\right)} = \frac{\frac{1}{\sigma\left(0,\nu,T_M^{\text{ex}}\right)}\int_0^\infty\frac{\partial B\left(\nu,T_M^{\text{ex}}\right)}{\partial T}d\nu}{\int_0^\infty\frac{1}{\sigma\left(0,\nu,T_M^{\text{ex}}\right)}\frac{\partial B\left(\nu,T_M^{\text{ex}}\right)}{\partial T}d\nu}. \tag{67c}$$

(Equation (65b) is equivalent to the result obtained by Morel *et al.* [7]; we have simply manipulated it into a different form.) The three results in Eqs. (65) obviously have the same form, which is remarkable in itself. In words, Eqs. (65) translate to the following:

> The boundary condition for the energy density is an integral over all frequencies and incident directions of a weight function times the incident intensity, and the weight function is the sum of two terms. The first term is a (temperature-dependent) constant times μ; the second is a temperature- and frequency-dependent function times μ^2.

We begin our comparison by considering the very simple case of a Planckian incident intensity:

$$F(\nu, \mu) = B(\nu, T_0) \qquad \text{and} \qquad F_{mg} = B_g(T_0).$$

Then we have $T_M = T_0$, and Eqs. (65) produce

$$\begin{aligned} ac\left(T_{1/2}^{(0)}\right)^4\Big|_{\text{SCB}} &= \sum_{g=1}^{G} \sum_{\mu_m>0} w_m \left[\frac{2\mu}{\rho}(2 - r_{\text{SCB}}) + 3\mu_m^2 q_{g,\text{SCB}}\right] B_g(T_0) \\ &= \sum_{g=1}^{G} [(2 - r_{\text{SCB}}) + q_{g,\text{SCB}}] B_g(T_0) \qquad (68a) \\ &= (2 - r_{\text{SCB}} + r_{\text{SCB}}) \frac{1}{2} ac(T_0)^4 = ac(T_0)^4, \end{aligned}$$

$$ac\left(T_{1/2}^{(0)}\right)^4\Big|_{\text{LLD}} = \sum_{g=1}^{G} [(2 - r_{\text{LLD}}) + q_{g,\text{LLD}}] B_g(T_0) = \cdots = ac(T_0)^4, \qquad (68b)$$

$$ac(T^{\text{var}})^4 = \int d\nu [(2 - r_{\text{var}}) + q_{g,\text{var}}] B(\nu, T_0) = \cdots = ac(T_0)^4. \qquad (68c)$$

(Here we have used the fact that the Planck-averaged $q_{g,X}$ equals r_X for $X = \text{SCB}$, LLD, and variational.) Thus, given a Planckian incident intensity, the leading-order interior solution produced by the discrete methods satisfies the correct Marshak boundary condition. This is as we would hope and expect.

In general, the most obvious difference between the discrete and variational results is that the discrete results replace integrals with summations. This suggests two conditions for accuracy:

(i) The quadrature set should accurately approximate two half-range integrals—μ times the incident intensity and μ^2 times the incident intensity—in each frequency group.

(ii) The group structure and group-averaged opacities should be chosen such that the group sum of F_{mg}/σ_g is an accurate approximation of the frequency integral of F/σ.

If we assume that the quadrature set and group structure meet these requirements, then the differences among the three boundary conditions are due to differences in their definitions of the two opacity ratios r and q, defined in Eqs. (65) and (66). To help gain an understanding of these differences we shall assume for the moment that the multigroup and quadrature sums can be replaced by the integrals they approximate, and we shall consider a simple

model opacity [12]:

$$\sigma(\nu, T) = \sigma_0 \frac{1 - \exp(-h\nu/kT)}{(h\nu)^3}. \tag{69}$$

This model opacity has two key characteristics of real opacities: it is much larger for $h\nu \ll kT$ than for $h\nu > kT$, and for a given $h\nu$ it decreases as T increases.

Given our model opacity we can explicitly evaluate q_{var},

$$q_{\text{var}}(\nu) = q_0 \frac{(h\nu/kT_M)^3}{1 - \exp(-h\nu/kT_M)}, \tag{70}$$

where q_0 is a constant whose numerical value is approximately 0.005. The most important feature of q_{var} is that it is vanishingly small for $h\nu \ll kT_M$ and very large for $h\nu \gg kT_M$. The same holds for q_{SCB} and q_{LLD}. As a result, if the incident intensity F is concentrated at frequencies ν such that $h\nu \ll kT_M$, then the term containing q in the boundary condition is negligible, and

$$\begin{aligned} ac(T^{\text{var}})^4 &\to (2 - r_{\text{var}}) \int d\nu \int_0^1 d\mu 2\mu F(\nu, \mu, t), \\ \Rightarrow \frac{(T^{\text{var}})^4}{(T_M)^4} &\to \frac{2 - r_{\text{var}}}{2}. \end{aligned} \tag{71}$$

Given the model opacity we can explicitly evaluate r_{var},

$$r_{\text{var}} = \frac{4}{7} \frac{2\zeta(6)}{\zeta(6) + \zeta(7)} \approx 0.57, \tag{72}$$

where ζ is the Reimann zeta function, $\zeta(n) \equiv \sum_{k=1}^{\infty} k^{-n}$.

Thus, given incident intensities concentrated at low frequencies, the boundary condition satisfied by the leading-order solution is lower than the Marshak boundary condition, and the ratio of the two does not depend on temperature or any details of the incident intensity F:

$$\frac{(T^{\text{var}})^4}{(T_M)^4} \xrightarrow[\text{low-}\nu \text{ incidence}]{} \frac{2 - r_{\text{var}}}{2} = \frac{3\zeta(6) + 7\zeta(7)}{7\zeta(6) + 7\zeta(7)} \approx 0.71. \tag{73}$$

(This is the case, at least, if Pomraning's variational result is a good approximation of reality.) Similar conclusions hold for the discrete methods,

$$\left.\frac{\left(T_{1/2}^{(0)}\right)^4}{(T_M)^4}\right|_{\text{SCB}} \to \frac{2 - r_{\text{SCB}}}{2}, \qquad \left.\frac{\left(T_{1/2}^{(0)}\right)^4}{(T_M)^4}\right|_{\text{LLD}} \to \frac{2 - r_{\text{LLD}}}{2}, \tag{74a,b}$$

although the ratios r_{SCB} and r_{LLD} are not constants, but depend on T_M and $T_{1/2}^{(0)}$. For example, given the model opacity, we can calculate

$$r_{\text{SCB}} = \frac{1 + \alpha + \alpha^2 + \alpha^3}{1 + \alpha + \alpha^2 + \alpha^3 + \alpha^4 + \alpha^5 + \alpha^6}, \qquad \alpha \equiv T_{1/2}^{(0)}/T_M. \tag{75}$$

(We have been unable to evaluate r_{LLD} analytically, even given our model opacity.) There is only one real positive α that satisfies both Eqs. (74a) and (75); we have found it numerically:

$$\alpha^4 = \left.\frac{\left(T_{1/2}^{(0)}\right)^4}{(T_M)^4}\right|_{\mathrm{SCB}} \xrightarrow[\text{low-}\nu\text{ incidence}]{} \approx 0.67. \tag{76}$$

This differs from the variational result, 0.71, by only 6%. Like the variational result, the SCB result is independent of temperature and details of the incident intensity.

While we were unable to analytically compute r_{LLD}, we did evaluate it numerically and found that it is very close to the SCB result—closer, in fact, than either result is to the variational result. Thus, we conclude the following.

(i) Pomraning's variational result implies that, given our model opacity, if the incident intensity at a boundary is concentrated at low frequencies (such that $h\nu \ll kT_M$), then the boundary condition satisfied by the leading-order interior energy density is approximately 71% of the Marshak value.

(ii) A similar result holds for SCB; the value is approximately 67%. (This assumes that the quadrature set accurately integrates μF over incident directions and that frequency-group sums are accurate approximations of frequency integrals.)

(iii) A similar result holds for LLD; the value is very close to that of SCB.

(iv) The above are true regardless of temperature, angular distribution of the incident intensity, or frequency distribution of the incident intensity, provided only that the incident frequencies are low enough.

(v) We do not know from our analyses how accurate Pomraning's variational estimate is. Numerical testing with very fine meshes is our only means of assessing this.

Our first series of test problems in the numerical-results section is designed to test these theoretical predictions, which, we remind the reader, hold only for incident intensities that are concentrated at low frequencies.

We turn next to incident intensities concentrated at intermediate frequencies such that the values of q_g are order 1. In such problems the directional distribution of the incident intensity plays a significant role in determining the boundary condition satisfied by the interior solution, because both a μ-weighted integral and a μ^2-weighted integral of the incident intensity are important. Obviously, in these problems the SCB boundary condition will be very close to Pomraning's variational approximation to the exact condition if r_{SCB} is close to r_{var} and q_{SCB} is close to q_{var}. Returning to our model opacity, and continuing to assume that the discrete sums are excellent approximations to the integrals, we can analytically compute a simple relationship between q and r in the variational and the SCB boundary conditions:

$$q_{\mathrm{var}}(\nu) = r_{\mathrm{var}}\left[\frac{\zeta(4)}{120\zeta(6)}\frac{(h\nu/kT_M)^3}{1-\exp(-h\nu/kT_M)}\right], \tag{77a}$$

$$q_{\mathrm{SCB}}(\nu) = r_{\mathrm{SCB}}\left[\frac{\zeta(4)}{120\zeta(6)}\frac{(h\nu/kT_M)^3}{1-\exp(-h\nu/kT_M)}\right] = \frac{r_{\mathrm{SCB}}}{r_{\mathrm{var}}}q_{\mathrm{var}}(\nu). \tag{77b}$$

We are unable to compute a similar analytic relationship between q_{LLD} and r_{LLD}; however, we have observed numerically that q_{LLD} is usually much closer to q_{SCB} than either is to q_{var}. Given this and Eq. (77b), the difference between the numerical methods' boundary

condition and the variational condition boils down to the difference between $r_{\rm SCB}$ and $r_{\rm var}$. Analytic expressions for these ratios (given the model opacity) are shown in Eqs. (72) and (75). The variational value is ≈ 0.57; the SCB value depends on the ratio of the boundary-condition temperature to the Marshak temperature. If that ratio were small, then $r_{\rm SCB}$ could approach unity, which is significantly different from $r_{\rm var}$. But how small can that ratio get? Note that

$$\alpha^4 \equiv \left(\frac{T_{1/2}^{(0)}}{T_M}\right)^4 = \frac{\int_0^\infty d\nu \int_0^1 d\mu \left[2\mu(2-r_{\rm SCB}) + 3\mu^2 q_{g,\rm SCB}\right] F(\mu,\nu)}{\int_0^\infty d\nu \int_0^1 d\mu [4\mu] F(\mu,\nu)}$$
$$> \frac{\int_0^\infty d\nu \int_0^1 d\mu [2\mu(2-r_{\rm SCB})] F(\mu,\nu)}{\int_0^\infty d\nu \int_0^1 d\mu [4\mu] F(\mu,\nu)} = \frac{2-r_{\rm SCB}}{2}. \tag{78}$$

(Here we continue to assume for simplicity that the discrete angle and frequency sums are roughly equal to the integrals they approximate.) Thus, the temperature ratio must be greater than that which satisfies $2\alpha^4 = 2 - r_{\rm SCB}$. We found above that the α^4 satisfying this equation is ≈ 0.67, which corresponds to $r_{\rm SCB} \approx 0.66$. This shows that the factor $r_{\rm SCB}/r_{\rm var}$ appearing in Eq. (77b) can never be larger than $\approx 0.66/0.57 \approx 1.16$ and that this limiting value is attained only if the q term it multiplies is unimportant! We conclude that *if the boundary-condition temperature is lower than the Marshak temperature the SCB boundary condition will be very close to the variational estimate obtained by Pomraning.*

If, on the other hand, the boundary-condition temperature is higher than the Marshak temperature, i.e., if $\alpha > 1$, then $r_{\rm SCB}$ could be significantly smaller than $r_{\rm var}$, which could potentially lead to significant error in the q term in the boundary condition. Let us examine how large α can be:

$$\alpha^4 \equiv \left(\frac{T_{1/2}^{(0)}}{T_M}\right)^4 = \frac{\int_0^\infty d\nu \int_0^1 d\mu \left[2\mu(2-r_{\rm SCB}) + 3\mu^2 q_{\rm SCB}(\nu)\right] F(\mu,\nu)}{\int_0^\infty d\nu \int_0^1 d\mu [4\mu] F(\mu,\nu)}$$
$$= \frac{2-r_{\rm SCB}}{2} + \frac{\int_0^\infty d\nu \int_0^1 d\mu \left[3\mu^2 (r_{\rm SCB}/r_{\rm var}) q_{\rm var}(\nu)\right] F(\mu,\nu)}{\int_0^\infty d\nu \int_0^1 d\mu [4\mu] F(\mu,\nu)}$$
$$< \frac{2-r_{\rm SCB}}{2} + \frac{3}{4}\frac{r_{\rm SCB}}{r_{\rm var}} \left[\sup_{\substack{\mu,\nu \text{ such that} \\ F \text{ is important}}} \{\mu q_{\rm var}(\nu)\} \right]$$
$$< 1 + r_{\rm SCB} \left(\frac{3}{4 \cdot 0.57} \sup_{\substack{\mu,\nu: F \text{ is} \\ \text{important}}} \{\mu q_{\rm var}(\nu)\} - \frac{1}{2} \right)$$
$$< 1 + \frac{1}{\alpha^3} \left(1.32 \sup_{\substack{\mu,\nu: F \text{ is} \\ \text{important}}} \{\mu q_{\rm var}(\nu)\} - \frac{1}{2} \right). \tag{79}$$

(Here we used the fact that $r_{\rm SCB} > 1/\alpha^3$ for finite positive α.) Clearly, α can become large only if $q_{\rm var}(\nu)$ becomes large. But our assumption at the moment is that q is order 1, which means that α cannot be much greater than unity. If α is not much greater than unity, then $r_{\rm SCB}$ will be close to $r_{\rm var}$, and therefore $q_{\rm SCB}$ will be close to $q_{\rm var}$. We conclude that if incident

intensities are concentrated at intermediate frequencies such that q is close to unity, the SCB solution will satisfy boundary conditions that are quite close to the variational estimate of the exact conditions.

Finally, we consider incident intensities concentrated at high frequencies such that $h\nu \gg kT_M$. It is clear from Eqs. (67c) and (70) that at these frequencies q_{var} can become very large, causing the $3\mu^2$ term to dominate the 2μ term in Eq. (65c). This can lead to boundary-condition temperatures much larger than the Marshak temperature. Further, as shown in Eq. (79), a large value of q also leads to a large α and thus to an $r_{\text{SCB}}/r_{\text{var}}$ ratio that is small, and hence to an SCB boundary condition that is significantly lower than the variational estimate. This effect would be maximized for normally incident intensities and minimized for grazing-angle incident intensities. However, this result is somewhat misleading, because it comes from an asymptotic analysis that assumes the problem is optically thick *at every frequency*. In reality, problems tend to be optically thin, or at least not very thick, at frequencies such that $h\nu \gg kT_M$. Thus, one must ask whether the analyses presented thus far have any bearing on problems with incident intensities at high frequencies. We address this question in Section V.

In summary, the boundary condition satisfied by the leading-order SCB solution is remarkably close to Pomraning's variational approximation of the exact boundary condition. Our studies using model opacities indicate that differences between the SCB and variational boundary conditions will usually be a few percent. Differences between boundary conditions satisfied by the SCB method (which uses half-cell opacities) and the LLD method (which uses opacities at cell-average temperatures) will usually be smaller. An exception could be cases in which the incident intensity is concentrated at frequencies $h\nu \gg kT_M$; for such problems the asymptotic analysis predicts that the SCB solution will satisfy a boundary condition that is smaller than that of the variational estimate. However, the asymptotic analysis is suspect in such problems. This is discussed further in Section V and tested numerically in Section VI.

One uncertainty in this analysis is the accuracy of the variational result to which we are comparing the discrete results. We can get some feel for this by studying one-group steady-state problems, for which the exact boundary condition can be obtained and compared against the variational result. In such problems the variational result can be in error by as much as 10% given an intensity incident at a grazing angle, but is within a few percent for most incident distributions. In the more realistic (energy-dependent, transient) case, the variational result cannot be any better than this and is probably worse. We can further explore this question by numerical experiment, and we do so in Section VI.

E. *Summary*

To summarize, our analysis predicts that the multigroup discrete-ordinates SCB method performs remarkably well on optically thick slabs (optically thick in every frequency group, strictly speaking) even when boundary layers are not resolved by the spatial grid and initial layers are not resolved by time steps. The leading-order solution has the correct angular and energy distributions, as we see by comparing Eqs. (33) and (8). In the interior of the slab the leading-order SCB temperature satisfies a reasonable and robust discretization (64) of the equilibrium diffusion equation (12) that the exact leading-order temperature solution satisfies. This solution satisfies an initial condition (52) that agrees closely with the exact condition (13), and boundary conditions (65a) that agree reasonably well with a variational estimate (65c) of the exact boundary conditions, at least in most cases.

V. PROBLEMS THAT ARE BOTH "THICK" AND "THIN"

In the preceding section we discussed an asymptotic analysis that assumed that the problem in question was optically thick for every frequency of interest. Here we consider the more realistic case in which the problem is not thick in the higher-frequency groups, but is thick in the others.

Consider an intensity incident on the left face of a slab ($x = 0$) that is not optically thick (less than or equal to a few mean-free paths) at the incident frequencies. We can decompose this problem into two simpler problems: one for the "uncollided" intensity and one for the "emitted" intensity. The uncollided intensity is

$$I_{\text{un}}(x, \nu, \mu) = F(\nu, \mu) \exp\left\{ -\int_0^x \sigma(\nu, T(x'))\, dx' \Big/ \mu \right\}, \tag{80}$$

which leads to the direct energy deposition:

$$Q(x) = \int_0^\infty d\nu\, \sigma(\nu, T(x)) \int_0^1 d\mu\, I_{\text{un}}(x, \nu, \mu). \tag{81}$$

The problem for the emitted intensity has no incident photons (i.e., vacuum boundaries); it is driven by the volumetric energy source given in Eq. (81). The asymptotic analysis is likely to apply to this problem, which means that the emitted intensity is likely to be Planckian (to leading order) at a material temperature that satisfies the equilibrium diffusion equation (12). In fact, we contend that the analysis *does* apply if the emitted intensity is concentrated mostly in frequencies for which the slab is optically very thick. Thus, we contend that if an incident intensity is concentrated at high frequencies, the leading-order solution is the sum of an uncollided component and a diffusive component. (Again, this assumes that the emitted intensity is concentrated in frequencies for which the slab is optically thick.) The uncollided component is given by Eq. (80) and the diffusive component by Eq. (12), with the source Q given by Eq. (81). This implies that the SCB and LLD methods will perform well on such problems, provided the cells are thin enough that SCB and LLD get the attenuation in Eq. (80) approximately right. This result is likely of more practical significance than the pure asymptotic-theory results, which required the assumption that the problem is optically thick for all frequencies of interest.

In the next section we will test these predictions using problems with high-frequency incident intensities.

VI. NUMERICAL RESULTS

In previous sections we made a variety of predictions about the behavior of discretized transport solutions in optically thick radiative-transfer problems. In this section we demonstrate this behavior by running a variety of test problems. We find that in every problem that meets the assumptions of the analysis, the numerical solution behaves as predicted. In particular, we find that the fully implicit multigroup discrete-ordinates SCB (FI/MG/DO/SCB) method is remarkably accurate, even given coarse spatial meshes that do not resolve boundary layers or wave fronts.

A brief discussion of our solution technique is in order. We used a fully implicit time discretization with the exception that opacities and specific heats were evaluated at

beginning-of-step temperatures. To obtain an implicit Planckian we used a Newton–Raphson iteration based on

$$B(T_{k+1}) \approx B(T_k) + (T_{k+1} - T_k)\frac{\partial B}{\partial T}\bigg|_{T_k}.$$

This leads to a linear steady-state multigroup transport problem to be solved (or approximately solved) for each Newton–Raphson iteration in each time step. We approximately solved each such problem by performing a single iteration using a one-group equation to accelerate the multifrequency iterations. Our overall iteration strategy for a given time step is as follows:

(i) Define T_0 as the temperature at beginning of time step. Make a reasonable guess for T_1.

(ii) Compute $B_g = B_g(T_{k-1}) + (T_k - T_{k-1})[\partial B_g/\partial T]_{k-1}$ in each half-cell and group.

(iii) With known B_g, solve for the intensity in each direction, half-cell, and group.

(iv) Compute an integrated-intensity residual.

(v) Solve a one-group problem for an additive correction to the integrated intensity [13]. (This problem requires iteration; we accelerate it using a transport-synthetic acceleration method [14].) Use new integrated intensity to get new matter temperature, T_{k+1}.

(vi) If T_{k+1} is close enough to T_k and the integrated intensity is close enough to its previous value, this ends the time step. Otherwise increment k and return to step (ii).

In the following subsections we present numerical and theoretical results from a variety of problems. This allows us to check many different aspects of the predictions of our theory and in the end to draw conclusions about the accuracy of the discretization scheme we employ. We shall begin in subsection A with several problems that employ our "model" opacity and thus test the detailed quantitative theoretical predictions that we made for such opacities. Subsection B is devoted to test problems with real-world opacities, with which we study boundary-layer effects using 15 different incident distributions. The final subsection considers a time-dependent problem with a wave front, examining the accuracy of a coarse-mesh solution as a function of time and position.

To judge the accuracy of the coarse-mesh solution, we compare its material temperature and radiation energy density against fine-mesh and/or theoretical results. We define the radiation energy density as

$$E_R(x,t) = aT_R^4(x,t) = \frac{1}{c}\int_0^\infty d\nu \int_{-1}^1 d\mu \psi(x,\mu,\nu,t).$$

Here we have also defined the "radiation temperature" (T_R) which is another convenient quantity to compare. When thermal equilibrium is reached and the radiation field is in a Planckian distribution, the radiation and material temperatures are equal.

A. *Steady-State Problems Using Model Opacities*

In Section IV.D, we made several sharp quantitative predictions under the assumption of the "model" opacity of Eq. (69). To test those predictions we consider a 1-cm slab with the constant σ_0 chosen such that the slab is quite optically thick in the low-frequency groups but only a few mean-free paths thick in the high-frequency groups. We generate multigroup

TABLE I
16-Group Opacities, Evaluated at kT = 0.1 keV

Group	$h\nu_{\text{high}}$ (keV)	Model opacity (cm^{-1})	SiO_2 opacity (cm^{-1})
1	1.7780e−2	9.1353e+7	6.2081e+5
2	3.1610e−2	2.2486e+7	5.5395e+5
3	5.6210e−2	5.9398e+6	4.9732e+5
4	1.0000e−1	1.4205e+6	4.1049e+5
5	1.7780e−1	3.0853e+5	2.9181e+5
6	3.1610e−1	6.5712e+4	1.5912e+5
7	5.6210e−1	1.5458e+4	5.4127e+4
8	1.0000e+0	3.8265e+3	3.1412e+4
9	1.7780e+0	8.2908e+2	2.4673e+4
10	3.1610e+0	1.6166e+2	1.2242e+4
11	5.6210e+0	3.0088e+1	2.2580e+3
12	1.0000e+1	5.4764e+0	3.9908e+2
13	1.7780e+1	9.8477e−1	6.7010e+1
14	3.1610e+1	1.7639e−1	1.0726e+1
15	5.6210e+1	3.1510e−2	2.8111e+0
16	1.0000e+2	5.6156e−3	2.5945e−1

Note. Group 1 starts at 0.01 keV.

cross sections by taking Rosseland averages of the model opacity over each group. We then consider three sets of test problems with non-Planckian incident frequency distributions that test three regimes of interest. In the first two sets of problems we employ 16 frequency groups, the cross sections for which are shown in Table I for $kT = 0.1$. In the first set of problems the incident energy is in the lowest-frequency group (1). In the second, the energy is in an intermediate group (6) such that $h\nu/kT_M$ is order 1. In the third set of test problems we employ 12 frequency groups, and the energy is incident in the highest group, for which $h\nu/kT_M \gg 1$ and the opacity is too small to satisfy the assumptions of the diffusion-limit analysis. In each case the incident intensity impinges on the left face of the slab, while the right face is reflecting.

A.1. Incident intensity in lowest-frequency group. If the incident intensity at a boundary is concentrated at low frequencies (such that $h\nu \ll kT_M$), then (given the model opacity) our theory predicts that the boundary condition satisfied by the leading-order interior energy density for SCB would be 67% of the Marshak value if there were no angular or frequency discretization. Given the 16 frequency groups of Table I and the S_{16} quadrature set, the prediction changes from 67% to approximately 64.5%. This result is predicted to be independent of the angular and frequency distribution of the incident intensity. Here we test these theoretical predictions.

We examine the coarse-mesh interior solution given incident intensities in group one (for which $h\nu \ll kT_M$) for three different angular distributions: normally incident, grazing-angle incident, and isotropic. In each case the incident intensity is normalized such that energy flow rate into the problem is equal to the flow rate from a Planckian incident intensity at a temperature of 0.1 keV—only the *distribution* of the incident energy is different. Thus, in each case the "Marshak" boundary-condition temperature is 0.1 keV. The theory predicts, then, that each problem will attain a boundary-condition temperature of $(0.645)^{1/4} \times 0.1$ keV,

TABLE II
Material Temperatures from Problems with Model Opacity

Incident spectrum	Angular distribution	T_m interior (predicted)	T_m interior (calculated)
Group 1	Isotropic	0.0896	0.0899
	Grazing	0.0896	0.0899
	Normal	0.0896	0.0899
Group 6	Isotropic	0.0914	0.0919
	Grazing	0.0898	0.0902
	Normal	0.0923	0.0929

or 0.0896 keV. Our coarse-mesh numerical results are presented in the first three rows of Table II. The value attained, 0.0899, is in excellent agreement with the asymptotic prediction of 0.0896, which we note is only the leading-order term in an asymptotic expansion of the solution. As the theory predicts, the value attained is completely independent of the angular distribution of the incident intensity. We remark that we obtained the same results when we direct the same energy flow rate into other low-frequency groups such that $h\nu \ll kT_M$ is satisfied. That is, our numerical experiments confirm the theoretical prediction that as long as the incident photons have $h\nu \ll kT_M$, the interior solution does not depend on the angular or frequency distribution of those photons, but only on the total energy flow rate. Our results also confirm the theoretical prediction that in this case the correct energy density is approximately 35% lower than the solution one would obtain from diffusion theory with a *Marshak* boundary condition.

Table II shows excellent agreement between numerical results and theoretical predictions, but it does not address the accuracy of the numerical solution. The accuracy in these problems was comparable to that in similar problems with real opacities, which are shown later—approximately 7% error for the grazing cases and $<2\%$ for the others. Also, this table does not address the interesting theoretical prediction that the coarse-mesh solution in the boundary half-cell will be inaccurate, taking on the "Marshak" value, even though the remainder of the solution is accurate. In all cases our numerical results do exhibit this behavior, and we give examples later in the subsection on problems with real opacities.

A.2. Incident intensity in group 6. If the incident intensity at a boundary is concentrated at intermediate frequencies (such that $h\nu \approx kT_M$), then (given the 16-group model opacity) our theory predicts that the boundary condition satisfied by the leading-order interior energy density for SCB would be 64.5% of the Marshak value *plus* an additional term that depends on the frequency and angular distribution of the incident intensity. [The additional term is the one with q_{SCB} in Eq. (65a).]

Here we examine the coarse-mesh interior solution given incident intensities in group 6 (for which $h\nu \approx kT_M$) for three different angular distributions: normally incident, grazing-angle incident, and isotropic. In each case the incident intensity is normalized such that energy flow rate into the problem is equal to the flow rate from a Planckian incident intensity at a temperature of 0.1 keV, which means the "Marshak" boundary-condition temperature is 0.1 keV. Our theoretical predictions [from the discrete version of Eq. (65a)] and our coarse-mesh numerical results are presented in the second three rows of Table II. The differences between numerical and predicted results are approximately 0.5%, which is

excellent, especially considering that the predictions are for the leading-order term in an asymptotic expansion. Note that with the energy coming in at higher frequencies than in the previous problems, we now see a dependence on the angular distribution of the photons. This dependence is smaller for group 5 and larger for group 7, etc., because q_{SCB} increases with frequency and thus plays an increasing role. See Eq. (65a).

A.3. Incident intensity in highest group. If the incident intensity at a boundary is concentrated at high frequencies (such that $h\nu \gg kT_M$), then the asymptotic theory alone is invalid, because significant radiant energy is contained in groups for which the problem is not extremely optically thick. In this case we turn to our theory of Section V, in which we view the radiation energy density as the sum of an uncollided component and an "emitted" component. Provided that the matter temperature does not become extremely high, the vast majority of the emitted photons will be in frequency groups for which the problem is optically thick. Thus, in this case the asymptotic analysis holds for the emitted component. We can analytically estimate the uncollided component, provided we can obtain a reasonable estimate of the opacities as a function of position in the uncollided photons' frequency groups. (This opacity depends on temperature, of course, which depends on the emitted component.)

In the Appendix we describe our analytic estimate of the solution of a problem in which the incident intensity is in a single direction in a single "thin" frequency group and the opacity is the "model" opacity of Eq. (69). In Fig. 2a we display results from such a problem in which the incident direction was the most normally-incident angle in the S_{16} quadrature set and the incident group was the 12th of 12. The figure compares the radiation energy densities from a coarse-mesh SCB calculation, a fine-mesh SCB calculation, and our

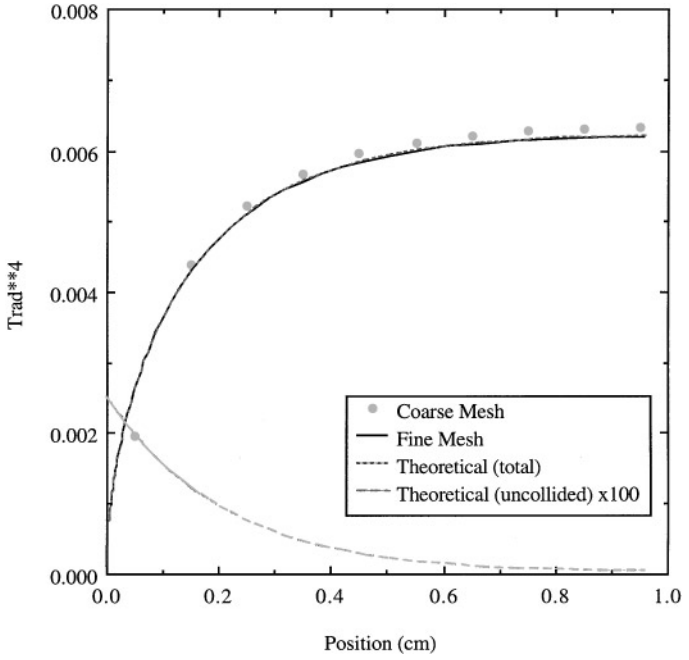

FIG. 2a. Theoretical, fine-mesh, and coarse-mesh results: normal incident in group 12 of 12. (The theoretical (total) curve is almost coincident with the fine-mesh curve.)

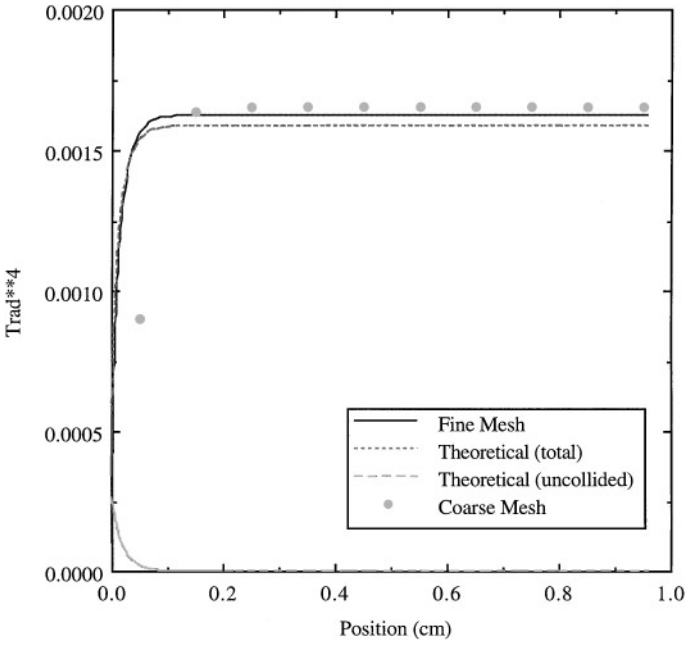

FIG. 2b. Fine-mesh and coarse-mesh results: grazing incident in group 12 of 12.

analytical estimate. The coarse-mesh solution is plotted using *cell-averaged* values plotted at *cell midpoints*. Agreement among the analytic, fine-mesh, and coarse-mesh solutions is clearly quite good. In Fig. 2b we present results from a similar problem, the difference being that the incident intensity is in the most grazing direction instead of the most normal. Again there is very good agreement between our theoretical prediction, a fine-mesh calculation, and a coarse-mesh calculation.

The agreement of our analytic estimates with the fine-mesh calculations in these problems strongly suggests that the theory developed in Section V is correct. The agreement with the coarse-mesh results supports the overall conclusion of this paper, based on both theory and numerical tests, that the FI/MG/DO/SCB discretization is a very robust method for radiative transfer calculations.

B. *Steady-State Problems with Real Opacities*

In the preceding section we considered several problems using an opacity that was an analytic function of frequency and temperature. This allowed us to make detailed quantitative comparisons between our theoretical predictions and numerical results. In this section we consider a series of test problems in which the opacities are "real" in the sense that they are approximately those of SiO_2, with a density chosen such that a 1-cm slab is optically very thick. Each problem was run in time-dependent mode until steady state was reached. Each problem employed an S_{16} Gauss–Legendre quadrature set, used the 16-group opacities described in Table I (which shows them at $kT = 0.1$ keV), and was subjected to a specified incident intensity on the left boundary and a reflecting condition on the right. The energy flow rate into each problem was equal to that from a Planckian incident intensity at a temperature $kT = 0.1$ keV. The only difference among the various problems was the frequency and direction distribution of the incident photons. (The "dilute Planckian" problems were

TABLE III

Comparison of Coarse-Mesh Radiation Energy Densities (J/cm^3) to Fine-Mesh Reference Solutions and "Marshak" Boundary Conditions, for Various Incident Distributions (Real Opacities)

Incident distribution		Energy density, surface			Energy density, interior			Marshak
Frequency	Direction	Reference	Coarse	% error	Reference	Coarse	% error	en. dens.
Planckian	Isotropic	1.372e+3	1.372e+3	0.0	1.372e+3	1.372e+3	0.0	1.372e+3
	Grazing	4.455e+3	1.372e+3	69.2	7.848e+2	8.413e+2	7.2	1.372e+3
	Normal	1.005e+3	1.372e+3	36.5	1.683e+3	1.663e+3	1.2	1.372e+3
Group 1	Isotropic	1.407e+3	1.372e+3	2.5	1.074e+3	1.091e+3	1.6	1.372e+3
	Grazing	4.485e+3	1.372e+3	69.4	7.479e+2	7.978e+2	6.7	1.372e+3
	Normal	1.036e+3	1.372e+3	32.4	1.257e+3	1.258e+3	0.04	1.372e+3
Group 6	Isotropic	1.384e+3	1.372e+3	0.87	1.226e+3	1.233e+3	0.7	1.372e+3
	Grazing	4.471e+3	1.372e+3	69.3	7.632e+2	8.196e+2	7.4	1.372e+3
	Normal	1.015e+3	1.372e+3	35.1	1.476e+3	1.464e+3	0.8	1.372e+3
Group 16	Isotropic	1.236e+3	1.306e+3	5.7	8.292e+5	8.559e+5	3.2	1.372e+3
	Grazing	4.267e+3	4.365e+3	2.3	1.088e+6	1.112e+6	2.3	1.372e+3
	Normal	7.776e+2	8.275e+2	6.4	6.754e+5	7.011e+5	3.8	1.372e+3
Dilute	Isotropic	8.401e+1	8.575e+1	2.1	1.129e+2	1.109e+2	2.4	8.575e+1
Planckian	Grazing	2.755e+2	8.575e+1	68.9	5.386e+1	5.776e+1	7.2	8.575e+1
	Normal	6.147e+1	8.575e+1	39.5	1.425e+2	1.387e+2	2.7	8.575e+1

exceptions: their energy flow rates were 1/16 the rates of the other problems.) For each problem, we obtained a reference solution using a 200-cell logarithmically spaced grid that resolved any boundary layers arising at the left boundary. The coarse-mesh SCB solutions were obtained using 10 equally spaced cells.

We consider five different frequency distributions, and for each of these we consider three different directional distributions, for a total of 15 different test problems. We summarize our results in Table III, which gives reference solutions, coarse-mesh solutions, and relative error between them, for two different spatial locations in each of the 15 problems. The "surface" quantity requires some explanation; in the reference case it is from the cell closest to the incident surface, which is essentially the surface quantity. In the coarse-mesh case, however, it is simply the left half-cell value from the first cell, which is the coarse-mesh version of a surface quantity. It is interesting to note that in all cases except the group-16 incident ones, this coarse-mesh surface solution is the Marshak boundary-condition value. This is exactly as predicted by the theory; see, for example, Eqs. (44). However, although this Marshak value is in considerable error relative to the reference surface value and relative to the reference interior value, this error does not propagate to the interior. For example, in the group-1 grazing case, this value is a factor of three lower than the reference surface energy density and a factor of almost two higher than the reference interior solution, yet the interior coarse-mesh solution errs by only 7%. Again, this is exactly what the theory predicts. To further illustrate the behavior of both the reference and coarse-mesh solutions in the presence of boundary layers, we later present plots of energy densities versus position for some of the more interesting cases.

We begin our discussion with the Planckian/isotropic incident intensity. The solution to this problem is that the intensity everywhere is a Planckian at 0.1 keV. Both the fine- and

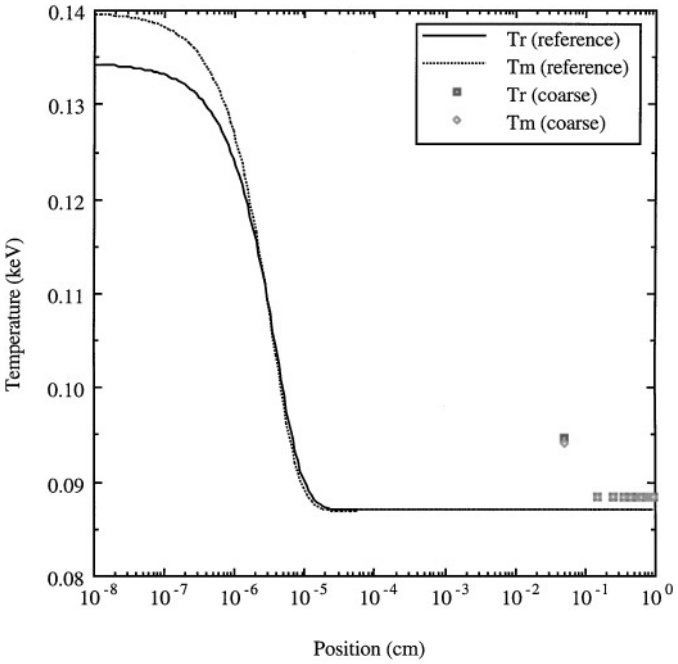

FIG. 3. Planckian/grazing-angle incident intensity, steady-state solution.

coarse-mesh solutions are exactly correct in this problem; it is essentially an infinite-medium problem and thus not a challenge to most spatial discretizations

The Planckian/grazing solution contains a boundary layer, as shown in Fig. 3. (Note the logarithmic spatial scale, which stretches the boundary layer out across most of the plot.) The interior solution in this problem is lower than that of the Planckian/isotropic solution, as predicted by the theory. This is easy to understand on physical grounds: more of the incident photons are now absorbed near the surface, which produces a higher temperature there, which causes a high rate of emission very close to the surface. Thus, more energy escapes this problem than the previous one. We see from the figure that the coarse mesh does not resolve the boundary layer at all, and thus cannot track the solution within that layer. Nevertheless, we see from the figure that the coarse-mesh solution is quite accurate in the interior of the problem. Turning to Table III, we see the numbers: the coarse-mesh solution at the surface is 69% low relative to the fine-mesh surface solution; in the interior, the coarse-mesh solution errs by only 7%. (We remark that a one-group steady-state linear problem with a grazing-angle incident intensity would yield approximately the same error, which in that simpler setting can be shown to stem from the difference between the variational-estimate and exact boundary conditions [3–5]. We believe that this is the source of the error here as well—that it is not caused by the nonlinearity, time dependence, or frequency dependence of the problem.)

The Planckian/normal solution also contains a boundary layer, as shown in Fig. 4. In this case, radiation penetrates deeper into the slab (on average) than in the isotropic case before being absorbed. This leads to lower emission losses from the surface and thus higher interior energy densities. We find again that the interior coarse-mesh solution is remarkably accurate—1.2% error—despite completely missing the boundary layer and missing the surface solution by 36%. If we explore why the normally incident coarse-mesh solution

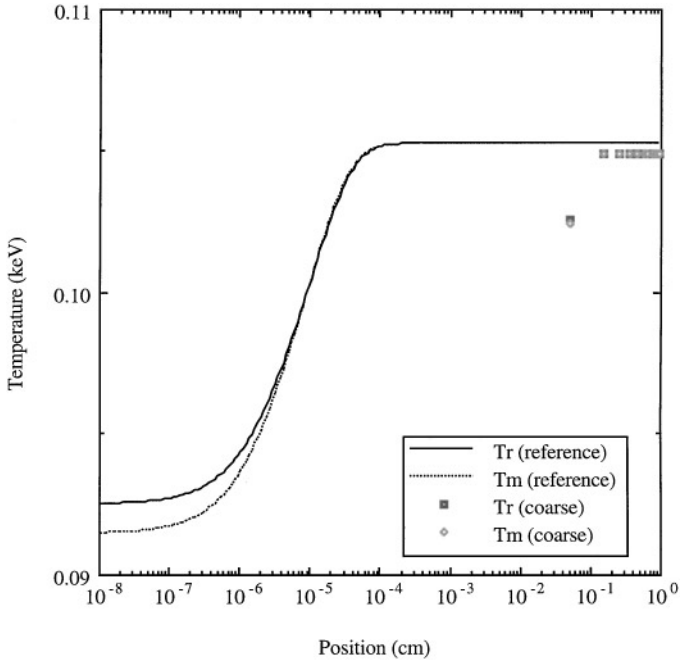

FIG. 4. Planckian/normal incident intensity, steady-state solution.

is more accurate than the grazing-incident, we eventually conclude that it is because the variational estimate is closer to the truth when μ is close to 1 than it is when μ is close to zero, not because the SCB boundary condition is closer to the variational condition.

We next consider an incident frequency distribution such that all photons appear in the lowest frequency group, group 1. In these problems, boundary layers develop at the left surface of the slab regardless of the incident directional distribution. The steepest boundary layer is in the grazing-angle problem, which minimizes the average distance from the boundary at which photons are absorbed and re-emitted, thus maximizing emission from the left surface (and the surface temperature) and minimizing the interior energy density. This is shown in Fig. 5. Returning to Table III, we find that the numbers are along the lines of the previous problems: the first coarse cell has temperatures and energy densities that are significantly lower than the correct surface quantities, but these errors do not propagate into the interior.

Continuing with the incident intensity in group 1, we next consider an incident direction that is almost normal to the surface (the direction in the S_{16} set whose cosine is closest to unity). Results from this problem are shown in Fig. 6. Note the nonmonotonic boundary layer that develops, and note that it begins and ends in the first one-thousandth of the first coarse cell, which means that the coarse mesh is ridiculously far from resolving it. Nevertheless, as predicted by theory, the coarse-mesh solution is extremely accurate in the interior. Again, of course, the coarse solution has significant error in the cell closest to the boundary, but this does not propagate into the interior.

We also considered an isotropic intensity incident in group 1. As one might expect, the solutions and errors were between those of the grazing and normally incident problems. In the boundary cell, where the coarse-mesh normally incident solution was too high and

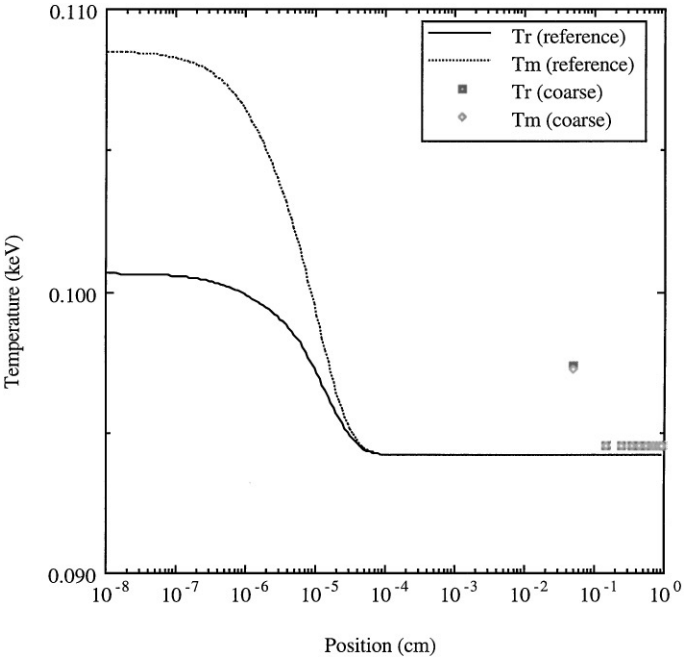

FIG. 5. Grazing-angle incident intensity into group 1, steady-state solution.

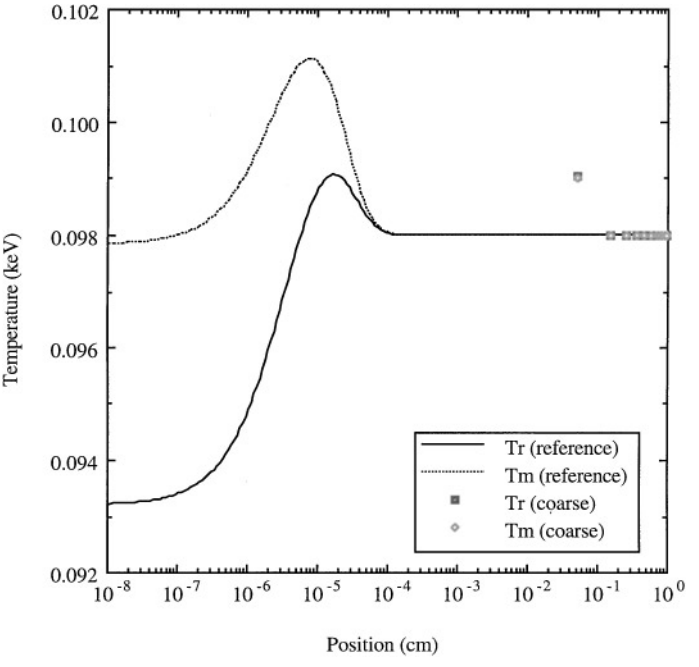

FIG. 6. Normal incident intensity into group 1, steady-state solution.

the grazing-incident solution too low, the isotropic-incident coarse-mesh solution has very little error. See Table III.

The next set of test problems has incident photons only in group 6. Coarse-mesh errors follow the same basic trends as in the group-1 problems, as shown in Table III. Interior solutions are generally higher in these problems than in the group-1 problems, because the incident photons penetrate farther on average before being absorbed, and thus fewer emitted photons are lost through the surface. Comparing the coarse-mesh and reference solutions, we again see that the coarse-mesh solutions have considerable error in the first cell but are remarkably accurate in the interior, as predicted by the theory.

Finally, we consider the case in which the incident intensity is concentrated at high frequencies. Here we do not expect the asymptotic theory to be correct, for the problem is not optically thick to high-frequency photons. However, as discussed previously, we expect the leading-order solution to be the sum of an uncollided component and an "emitted" component, with the asymptotic theory applying to the "emitted" component if the emitted intensities see the slab as very thick. Furthermore, the uncollided solution should be well represented by a coarse grid if the cell size is sufficiently fine (in high-frequency mfps) to represent the attenuation of the incident intensity.

Given that the incident intensity is deposited in the highest-frequency group (group 16), our numerical results indicate that the coarse grid solution is extremely accurate in the interior of the slab. Referring to Table III, the errors in the radiation energy density are $<4\%$ for the three angular distributions and the errors in the material temperature are $<1\%$.

In Fig. 7 we examine the grazing-angle incident case which shows that the interior temperature is much larger than T_M (which is 0.1 keV), indicating a very important uncollided component. The coarse mesh zone width, which is <0.4 mfps in group 16, accurately

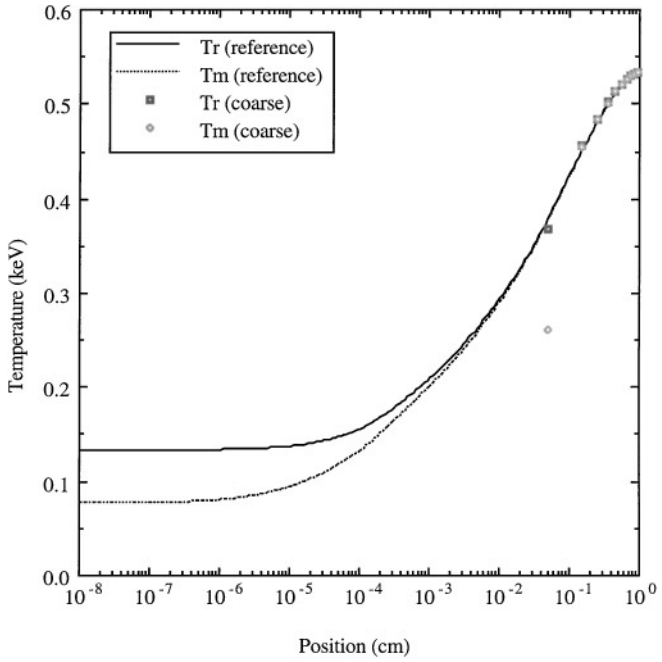

FIG. 7. Grazing-angle incident intensity into group 16, steady-state solution.

resolves this uncollided component and thus obtains an accurate source of emitted photons. As detailed in our "thick/thin" theory, this is all that is needed for the method to obtain an accurate coarse-mesh solution.

In practical applications it is sometimes the case that the source of radiation is some distance from the target of interest such that the target sees a "dilute" Planckian frequency spectrum. In our final set of steady-state problems we let the incident intensity equal a constant (1/16) multiplied by $B(\nu, T_0)$, with $T_0 = 0.1$ keV. The errors we see in Table III for this dilute Planckian incident spectrum are comparable to those in previous cases.

D. *Transient Problems*

Finally, we show a transient problem to illustrate that the FI/MG/DO/SCB method is accurate even when the mesh does not resolve wavefronts. We compare the time evolution of the solution for the case of a monoenergetic source incident on a 1-cm slab. For this transient problem, the specified incident flux is on the left boundary and a vacuum is on the right boundary. The radiation transport is modeled with the SCB spatial discretization, 12 energy groups (again using the SiO_2 opacities), and an S_8 quadrature set. The reference solution is obtained by resolving the boundary layers [at both boundaries] for all photon energy groups, using 1000 cells in each of the intervals: $0 < x < 0.001$, $0.001 < x < 0.999$, and $0.999 < x < 1.0$. The reference grid also resolves the wavefront away from boundaries. We obtained "coarse-mesh" solutions using 10 equally spaced cells. To measure the accuracy of the coarse mesh solution, we have compared the energy-integrated radiation intensity against the reference solution at three times during the transient.

This is a fully nonlinear problem in that the opacities are updated at every time step based on the latest estimate of the material temperature, and it is therefore a very rigorous test of the SCB method. In this time-dependent scenario we ask, given only the same initial and boundary conditions, whether the SCB scheme using a coarse mesh produces accurate results during the transient phase. In Fig. 8 we plot the spatial distribution of the integrated radiation intensity at three different times during the heating of the slab. We observe remarkable agreement with the reference solution for the interior points—errors are <6%—despite large errors at the left boundary [about 45%]. [We have plotted only cell-averaged quantities from the coarse-mesh solution.] Errors in the material temperature are also high for the left boundary point (about 20%), but are only about 2% for interior points. These results demonstrate that even with a very coarse grid (that does not resolve the boundary layers) we obtain excellent time-dependent results in the interior of the problem.

VII. DISCUSSION

This paper was motivated by the need to obtain accurate numerical solutions to (nonlinear) radiative transfer problems. Toward that end we have analyzed and tested a particular numerical method for radiative transfer problems in which the photon intensity is a function of one spatial coordinate, one direction variable, frequency, and time. The method discretizes the spatial variable using a subcell-balance method called SCB, the direction variable using the discrete-ordinates method, the frequency variable using the multigroup approximation, and the time variable using a method that is essentially fully implicit (FI/MG/DO/SCB for short).

Our choice of spatial discretization was motivated by the excellent behavior of the SCB/discrete-ordinates method in thick, diffusive, one-group, steady-state problems [9,10].

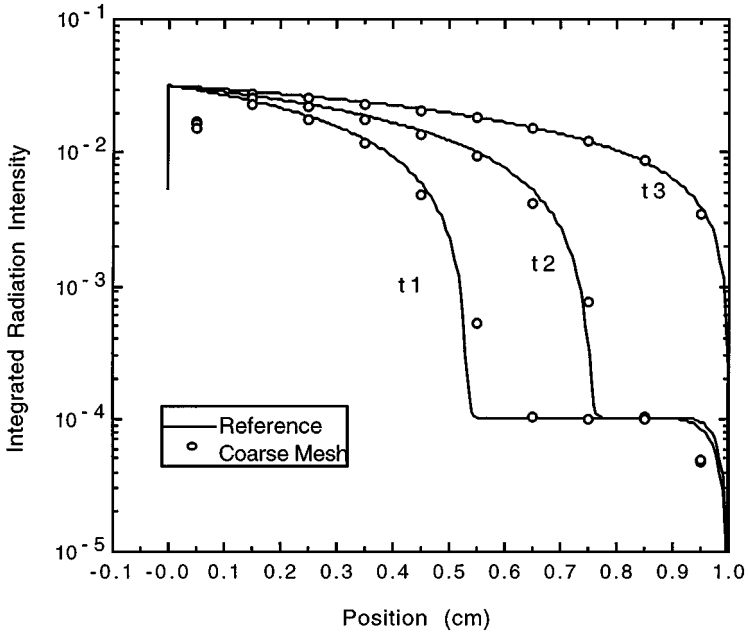

FIG. 8. Spatial distribution of integrated radiation intensity at three times [t1, t2, t3] during the heating of a slab by a monoenergetic beam of radiation incident at a grazing angle. The vertical line segment at $x = 0$ is actually the solution in the boundary layer.

SCB is less accurate away from the thick diffusive limit, even in one-group steady-state problems [10,11], so it is not the final answer to spatial discretization of radiative transfer problems. (It does have second-order truncation error in the fine-mesh limit, but its intermediate-mesh performance is relatively poor.) However, it is possible to develop related spatial discretizations that produce the SCB solution in thick diffusive regions but perform much better in other limits [10,11]. Thus, we study the comparatively simple FI/MG/DO/SCB method not only for its own intrinsic interest, but also for its impact on the development and understanding of other (more complicated and more accurate) spatial discretizations that behave like SCB in the thick diffusive limit.

Our analysis and results indicate that if a problem is optically thick in all frequency groups that contain significant radiant energy, the FI/MG/DO/SCB method is quite accurate. This is true, remarkably, even when there are sharp boundary layers that are not resolved by the spatial grid. Our analysis and results further indicate that if a problem is optically thin in frequency groups populated by the incident intensity, but thick to photons that are emitted by the matter in the problem, the numerical method is again quite accurate. We emphasize that our analyses and results apply to realistic problems—there were no simplifications made, for example, to remove the nonlinearity. The most significant simplifying factor is that we considered only one spatial dimension.

The results in this paper complement and extend those recently obtained by Morel *et al.* [7]. The SCB scheme analyzed here is slightly different from the LLD scheme analyzed by Morel *et al.* in that it uses two different opacities per cell; our results show that this leads to slight (but not significant) differences in the two methods' performances on unresolved boundary layers. We have also analyzed the initial layer, showing that the FI/MG/DO/SCB

method performs well even with unresolved initial layers. Since this analysis did not depend on having two opacities per cell, it holds also for the FI/MG/DO/LLD method. Our analysis of the SCB and LLD performances on unresolved boundary layers led to sharp quantitative predictions for a variety of scenarios; a large suite of detailed numerical calculations confirmed all of these predictions. We also included transient test problems with unresolved wavefronts, showing that the robustness of the FI/MG/DO/SCB scheme holds for such problems (which basically have moving boundary and initial layers). Finally, we included the first asymptotic analysis, to our knowledge, of radiative transfer problems that are optically thin in some frequency groups but optically thick in others. Our theoretical predictions were quite sharp, including an analytic solution of problem with model opacities, and were precisely confirmed by numerical testing.

The results presented here and by Morel *et al.* suggest several areas for further study. First, given that the most significant simplification here was the assumption of 1D slab geometry, a logical next step is to extend our analyses to multidimensional problems. We are actively pursuing this. Second, this analysis should be applied to other discretization schemes that have been used or proposed for radiative transfer. Third, the analysis should be extended to examine the radiation intensity that is *emitted* from optically thick slabs. Although the present analysis is silent on this subject, we are sure that the intensity emitted from the surface at an unresolved boundary layer has an incorrect distribution in frequency and direction. Further research should be able to quantify this.

APPENDIX

Analytic Estimate of Solution in Thick/Thin Problem

In this Appendix we describe our technique for analytically solving (with one approximation) a multigroup radiative transfer problem that is driven by a monodirectional beam in a high-frequency group—a group for which the problem is not very optically thick. The basic idea is to recognize that the radiation intensity has two components: an uncollided component and an "emitted" component. The emitted photons are likely to be in frequency groups for which the problem is optically thick; further, this emission source varies on the scale of a high-frequency mean-free path, which we assume is resolved by the spatial grid. Thus, the asymptotic diffusion-limit analysis developed in the body of this paper should apply to the emitted component.

The problem we wish to solve is

$$\mu_m \frac{\partial \psi_{m,g}}{\partial x} + \sigma_g(T(x))\psi_{m,g}(x) = \sigma_g(T(x))B_g(T(x)), \tag{A1.a}$$

$$2\sum_g \sigma_g(T(x))B_g(T(x)) = \sum_g \sigma_g(T(x)) \sum_m w_m \psi_{m,g}(x), \tag{A1.b}$$

$$\psi_{m,g}(0) = I_0, \text{ for } m = m_0 \text{ and } \mu_m > 0, \text{ and for } g = g_0 = \text{high-frequency group}, \tag{A1.c}$$

$$\psi_{m,g}(X) = \psi_{n,g}(X), \qquad \mu_m = -\mu_n < 0, \text{ all } g. \tag{A1.d}$$

We begin with expressions for the uncollided intensity:

$$\psi^u_{m_0,g_0}(x) = I_0 \exp\left\{ -\int_0^x dx' \sigma_{g_0}(T(x'))/\mu_{m_0} \right\}, \tag{A2.a}$$

$$\psi^u_{n_0,g_0}(x) = I_0 \exp\left\{ -\left[\int_0^x dx' \sigma_{g_0}(T(x')) + \int_x^X dx' \sigma_{g_0}(T(x')) \right] \Big/ \mu_{m_0} \right\},$$
$$n_0 : \mu_{n_0} = -\mu_{m_0}. \quad \text{(A2.b)}$$

The emitted component satisfies

$$\mu_m \frac{\partial \psi^e_{m,g}}{\partial x} + \sigma_g(T(x)) \psi^e_{m,g}(x) = \sigma_g(T(x)) B_g(T(x)), \quad \text{(A3.a)}$$

$$2 \sum_g \sigma_g(T(x)) B_g(T(x)) = \sum_g \sigma_g(T(x)) \sum_m w_m \psi^e_{m,g}(x) + \sigma_{g_0}(T(x)) w_{m_0} \left[\psi^u_{m_0,g_0}(x) + \psi^u_{n_0,g_0}(x) \right], \quad \text{(A3.b)}$$

$$\psi^e_{m,g}(0) = 0, \qquad \mu_m > 0, \text{ all } g, \quad \text{(A3.c)}$$

$$\psi^e_{m,g}(X) = \psi^e_{m,g}(X), \qquad \mu_m = -\mu_n < 0, \text{ all } g. \quad \text{(A3.d)}$$

The desired solution is the sum of the emitted and uncollided intensities.

We shall assume that the temperature distribution in the slab is such that the emitted photons are primarily in frequency groups for which the slab is optically thick. In this case the asymptotic analysis developed in this paper applies to the emitted component, and we find that the leading-order emitted component is Planckian,

$$\psi^{e(0)}_{m,g}(x) = B_g\left(T^{(0)}(x)\right), \quad \text{(A4)}$$

where the leading-order temperature satisfies an equilibrium diffusion equation:

$$-\frac{d}{dx} \frac{ac}{3\sigma_R\left(T^{(0)}(x)\right)} \frac{d\left[\left(T^{(0)}(x)\right)^4\right]}{dx} = \sigma_{g_0}\left(T^{(0)}(x)\right) w_{m_0} \left[\psi^u_{m_0,g}(x) + \psi^u_{n_0,g}(x) \right]. \quad \text{(A5)}$$

[The subscript R on the opacity denotes the Rosseland mean.] The boundary conditions are that the leading-order temperature goes to zero at $x = 0$ and its derivative with respect to x goes to zero at $x = X$.

If we can solve for the uncollided intensity and then somehow solve the equilibrium diffusion equation for the leading-order temperature, we will have solved the entire problem.

We shall make one approximation in our solution of Eq. (A2) for the uncollided intensity:

$$\exp\left\{ -\int_0^x dx' \sigma_{g_0}(T(x'))/\mu_{m_0} \right\} \approx \exp\left\{ -\sigma_{g_0}(\bar{T}) x/\mu_{m_0} \right\} \equiv \exp\left\{ -\bar{\sigma}_{g_0} x/\mu_{m_0} \right\}. \quad \text{(A6)}$$

That is, for purposes of computing the incident intensity, we shall use a constant opacity evaluated at some average temperature. Then we obtain

$$\begin{aligned} \left[\psi^u_{m_0,g}(x) + \psi^u_{n_0,g}(x) \right] &= I_0 \left[e^{-\bar{\sigma}_{g_0} x/\mu_{m_0}} + e^{-\bar{\sigma}_{g_0}(X+X-x)/\mu_{m_0}} \right] \\ &= I_0\, e^{-\bar{\sigma}_{g_0} X/\mu_{m_0}} \left[e^{\bar{\sigma}_{g_0}(X-x)/\mu_{m_0}} + e^{-\bar{\sigma}_{g_0}(X-x)/\mu_{m_0}} \right] \\ &= 2 I_0\, e^{-\bar{\sigma}_{g_0} X/\mu_{m_0}} \cosh\left(\frac{\bar{\sigma}_{g_0}(X-x)}{\mu_{m_0}} \right). \end{aligned} \quad \text{(A7)}$$

We shall now solve Eq. (A5), the equilibrium diffusion equation, with Eq. (A7) substituted on the right-hand side. At this point we must assume something about the opacities, and as described in the body of the paper, we assume a model opacity of the form

$$\sigma(\nu, T) = \rho\sigma_0 \frac{1 - e^{-h\nu/kT}}{(h\nu)^3}. \tag{A8}$$

Given this functional form, and assuming that the multigroup structure is fine enough that group sums accurately approximate their respective integrals, we have for the Rosseland mean

$$\sigma_R(T) = \frac{\int_0^\infty d\nu \frac{\partial B(\nu,T)}{\partial T}}{\int_0^\infty d\nu \frac{1}{\sigma_R(\nu,T)} \frac{\partial B(\nu,T)}{\partial T}} = \cdots = \frac{\frac{k}{h}(kT)^3 4!\zeta(4)}{\frac{1}{\rho\sigma_0}\frac{k}{h}(kT)^6 7!\frac{1}{2}(\zeta(6)+\zeta(7))}, \tag{A9}$$

where $\zeta(j)$ is the Reimann zeta function:

$$\zeta(j) = \sum_{n=1}^{\infty} \frac{1}{n^j}. \tag{A10}$$

We can simplify Eq. (A9) to find

$$\frac{1}{\sigma_R(T)} = \frac{1}{\rho\sigma_0} \frac{(kT)^3 7!(\zeta(6)+\zeta(7))}{4!2\zeta(4)} = \frac{1}{\rho\sigma_0}(210)(0.9358\ldots)(kT)^3. \tag{A11}$$

We use the chain rule to find

$$\frac{dT^4}{dx} = \frac{dT^4}{dT^7}\frac{dT^7}{dx} = \frac{d(T^7)^{4/7}}{dT^7}\frac{dT^7}{dx} = \frac{4}{7}(T^7)^{4/7-1}\frac{dT^7}{dx} = \frac{4}{7}T^{-3}\frac{dT^7}{dx}. \tag{A12}$$

We combine Eqs. (A11) and (A12),

$$\frac{ac}{3\sigma_R(T)}\frac{dT^4}{dx} = \frac{1}{\rho\sigma_0}(ac)(210)(0.9358\ldots)\,k^3\frac{4}{7}\frac{dT^7}{dx} = A\frac{dT^7}{dx}, \tag{A13}$$

where

$$A \equiv \frac{ack^3}{\rho\sigma_0}(120)(0.9358\ldots). \tag{A14}$$

Now if we put everything together, our equilibrium diffusion equation becomes

$$-\frac{d^2}{dx^2}\left[\left(T^{(0)}(x)\right)^7\right] = \frac{1}{A}\sigma_{g_0}\left(T^{(0)}(x)\right) w_{m_0} 2I_0\, e^{-\bar{\sigma}_{g_0}X/\mu_{m_0}} \cosh\left(\frac{\bar{\sigma}_{g_0}(X-x)}{\mu_{m_0}}\right). \tag{A15}$$

We shall once again invoke the approximation that the group-g_0 opacity is replaced by a suitable average, which we call $\bar{\sigma}_{g_0}$. The boundary conditions on the solution, which is now the leading-order temperature to the seventh power, are that it vanishes at $x = 0$ and its x-derivative vanishes at $x = X$. The solution is not difficult to obtain; it is

$$\left(T^{(0)}(x)\right)^7 = \frac{2}{\bar{\sigma}_{g_0}A} w_{m_0}\mu_{m_0}^2 I_0\, e^{-\bar{\sigma}_{g_0}X/\mu_{m_0}}\left[\cosh\left(\frac{\bar{\sigma}_{g_0}X}{\mu_{m_0}}\right) - \cosh\left(\frac{\bar{\sigma}_{g_0}(X-x)}{\mu_{m_0}}\right)\right]. \tag{A16}$$

We employed this expression in a spreadsheet and took its (1/7)th power to obtain our analytic estimate of the leading-order temperature in the slab. The expression depends on the average opacity, $\bar{\sigma}_{g_0}$, so to begin we simply inserted σ_{g0} evaluated at some reasonable temperature. At that point everything was known and we could plot the uncollided energy density, the emitted energy density, the total radiation energy density, and the matter temperature as functions of position. Given the matter temperature distribution, we improved our estimate of an average temperature at which to evaluate σ_{g0} and re-generated the plots. (The plots were not very sensitive to the temperature we chose for $\bar{\sigma}_{g_0}$, so this iteration converged quickly.) This is how Figs. 2a and 2b were generated.

ACKNOWLEDGMENTS

Work by the first author (M.L.A.) was supported by NSF Grant CCR-9302782. Work by the second author (P.F.N.) was performed under the auspices of the U.S. Department of Energy under Contract W-7405-Eng-48.

REFERENCES

1. E. W. Larsen, G. C. Pomraning, and V. C. Badham, Asymptotic analysis of radiative transfer problems, *J. Quant. Spectrosc. Radiat. Transfer* **29**, 285 (1983).
2. E. W. Larsen, The asymptotic diffusion limit of discretized transport problems, *Nucl. Sci. Eng.* **112**, 336 (1992).
3. E. W. Larsen and J.E. Morel, Asymptotic solutions of numerical transport problems in optically thick, diffusive regimes, II, *J. Comput. Phys.* **83**, 212 (1989); see also Corrigendum, *J. Comput. Phys.* **91**, 246 (1990).
4. M. L. Adams, Discontinuous finite-element transport solutions in the thick diffusion limit in Cartesian geometry, in *Proc. International Conf. on Advances in Mathematics, Computation, and Reactor Physics, Pittsburgh, PA, April 28–May 1, 1991* (1991), Vol. 5, p. 21.1 3-1.
5. M. L. Adams, T. A. Wareing, and W. F. Walters, Characteristic methods in thick diffusive problems, *Nucl. Sci. Eng.* (to appear).
6. M. L. Adams, E. W. Larsen, and P. F. Nowak, The asymptotic diffusion limit of continuous and discrete steady-state multigroup radiative transfer problems, in *Proc. Int. Conf. Advances in Mathematics and Computation, Reactor Physics, and Environmental Analysis, April 30–May 4, Portland, OR* (1995), Vol. 1, p. 360.
7. J. E. Morel, T. A. Wareing, and K. Smith, A linear-discontinuous spatial differencing scheme for *Sn* radiative transfer calculations, *J. Comput. Phys.* **128**, 445 (1996).
8. G. C. Pomraning, A variational treatment of the mixed boundary condition for the equilibrium diffusion equation, *J. Quant. Spectrosc. Radiat. Transfer* **36**, 471 (1986).
9. M. L. Adams, A new transport discretization scheme for arbitrary spatial meshes in XY geometry, in *Proc. ANS Topical Meeting, Advances in Mathematics, Computations, and Reactor Physics, Pittsburgh, April 29–May 2, 1991* (1991), Vol. 3, Sec. 13.2, p. 2-1.
10. T. L. Eaton and M. L. Adams, A new corner-balance/linear-discontinuous method for transport in slab geometry, *Trans. Amer. Nucl. Soc.* **70**, 158 (1994).
11. M. L. Adams, Subcell balance methods for radiative transfer on arbitrary grids, *Transport Theory Statist. Phys.* **26**, 385 (1997).
12. G. C. Pomraning, *The Equations of Radiation Hydrodynamics* (Pergamon, Oxford, 1973).
13. E. W. Larsen, A Grey transport acceleration method for time-dependent radiative transfer problems, *J. Comput. Phys.* **78**, 459 (1988).
14. G. L. Ramoné, M. L. Adams, and P. F. Nowak, Transport-synthetic acceleration methods for transport iterations, *Nucl. Sci. Eng.* **125**, 257 (1997).